AD NUMBER

AD893125

NEW LIMITATION CHANGE

TO

Approved for public release, distribution unlimited

FROM

Distribution authorized to U.S. Gov't. agencies only; Test and Evaluation; 15 Mar 1972. Other requests shall be referred to Space and Missile Systems Organization, Los Angeles AFS, CA.

AUTHORITY

SAMSO ltr, 17 Aug 1976
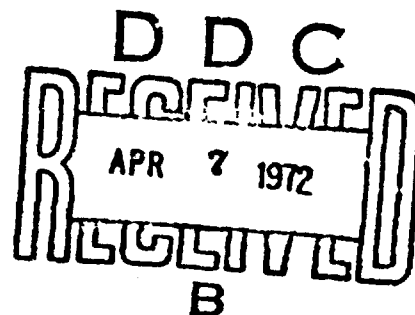
225-400 MHz Antenna System for Spin-Stabilized Synchronous Satellites

Prepared by H. E. KING and J. L. WONG
Electronics Research Laboratory
Laboratory Operations

D D C

RECEIVED

72 MAR 15

APR 7 1972

B

UB

Systems Engineering Operations
THE AEROSPACE CORPORATION

225-400 MHZ ANTENNA SYSTEM FOR SPIN-STABILIZED SYNCHRONOUS SATELLITES,

Prepared by

H. E. King and J. L. Wong
Electronics Research Laboratory
Laboratory Operations

72 MAR 15

Systems Engineering Operations
THE AEROSPACE CORPORATION

Prepared for

SPACE AND MISSILE SYSTEMS ORGANIZATION
AIR FORCE SYSTEMS COMMAND
LOS ANGELES AIR FORCE STATION
Los Angeles, California

FOREWORD

Approved

A. H. Silver, Director
Electronics Research Laboratory
Laboratory Operations

H. F. Meyer
Systems Engineering Director
Group II Programs
Satellite Systems Division
Systems Engineering Operations

Walter W. Sanders
Col., United States Air Force
Deputy for Space Communications
Systems

ABSTRACT

A wideband, circularly polarized antenna system has been developed for use on spin-stabilized synchronous satellites. The satellite is assumed to be a right-circular cylinder of 84-in. diam and 77.3-in. height. The antenna consists of two circular arrays of 12 radiating elements equally spaced around the circumference of the satellite. The axial spacing between the two arrays is 40 in. The basic radiating element is a crossed dipole with flat open sleeves, and the VSWR is less than 2.5:1 over a 1.8:1 frequency band (225 to 400 MHz). Both the dipoles and sleeves are of wire-grid construction for minimization of solar cell shadowing. The electrical performance of the antenna is established on the basis of half-scale model measurements. It is shown that the antenna can provide an EOE gain (gain in the direction of the edge of the earth) of more than 9.3 dB from 225 to 250 MHz and at least 8.5 dB from 250 to 400 MHz.

CONTENTS

PRECEDING PAGE BLANK--NOT FILMED

FIGURES

FIGURES (cont.)

TABLES

I. INTRODUCTION

The objectives of this study were the development and experimental demonstration of the RF feasibility of a wideband, circularly polarized antenna system for use on spin-stabilized satellites at synchronous altitude. The antenna system is required to operate over a frequency range of 225 to 400 MHz, and sufficient antenna gain must be provided in the direction of the edge of the earth (EOE). The general electrical performance requirements are summarized in Section IIA.

The satellite is assumed to be a right-circular cylinder of 84-in. diam and 77.3-in. height. In order to meet the bandwidth and gain requirements, the recommended antenna configuration is a two-bay, circular array of open-sleeve dipoles. Each array consists of 12 elements equally spaced around the circumference of the satellite, and the axial spacing between the two arrays is 40 in. Since the entire surface of the satellite is covered with solar cells, shadowing of the solar cells by the antenna must be minimal. For this reason, the dipoles and sleeves are of wire-grid construction. Clear quartz is recommended for the sleeve and dipole supports.

A half-scale model was used for evaluation of the electrical performance of the antenna. Pattern and directivity measurements were made over the 450 to 800 MHz frequency band. An axial dipole spacing of 20 in. and a dipole-to-reflector spacing of 5 in. were used for most of the measurements. However, measurements were also made with other spacings in an effort to optimize the array performance. Results of these measurements are discussed in Section III. On the basis of the measured pattern and directivity characteristics of the half-scale model, the electrical performance of a full-scale antenna has been projected, and the results have indicated satisfactory compliance with the specified gain requirements. The EOE gain is greater than 9.3 dB from 225 to 250 MHz and at least 8.5 dB from 250 to 400 MHz. A detailed discussion of the full-scale antenna configuration is given in Section IV.

-1-

II. DESCRIPTION OF ANTENNA SYSTEM

A. REQUIREMENTS AND DEVELOPMENT CONCEPT

The proposed antenna system is intended for use on spin-stabilized satellites that operate at synchronous equatorial orbit with the spin axis parallel to the earth's North-South pole. As previously mentioned, the spacecraft is assumed to be a right-circular cylinder of 84-in. diam and 77.3-in. height. Because the entire cylindrical surface is covered with solar cells, minimal shadowing of the solar cells by the antenna is an important consideration.

The antenna is an electronically despun antenna, and there are no strict requirements on the antenna beam shape and sidelobe levels. However, the gain levels must be met and circular polarization is required. The gain specifications at the earth's limb for the antenna system are given in Table 1. The gain includes all the losses associated with the antenna system but does not include the diplexer losses.

Table 1. Antenna Gain Specifications

Frequency, MHz	Gain at Earth's Limb, dBi
225-250	9.0
250-400	6.0
250-350	6.0 minimum

The antenna configuration is an array of crossed, open-sleeve dipoles capable of electronically switching the beam through 24 different positions equally spaced around the satellite's equator. Twenty-four crossed sleeve-dipoles are arranged to form two circular arrays of 12 elements equally spaced about the circumference of the satellite. The two circular arrays

are spaced 40 in. apart in the axial direction. The antenna beam is electronically despun, and only a 2 × 2 array is excited at any one time. The dipoles are fed in a similar manner as in the LES-6 antenna system (Refs. 1 and 2). When two adjacent pairs (2 × 2 array) of crossed dipoles are excited, a directive, circularly polarized radiation pattern is formed with the beam peak normal to the spin axis. By means of electronic sequential switching and phasing, as in the LES-6 system, the beam is scanned through 24 equally spaced position. A sensor-controlled switching logic points the beam toward the earth as the satellite rotates. In order to obtain two beams from two adjacent antennas, a difference of phase is applied between the signals at the two antennas. By reversing the phases of the two antenna signals, the beam can be scanned to another position. By successively switching a phase delay between the antennas, e.g., ± 25 deg, a beam can be generated every 15 deg. No adjacent pair is ever fed in phase because the proper delay is inserted to scan the beam ±7.5 deg about the in-phase position. The two beams generated from two adjacent antennas, the beam switching locations, and the beam positions relative to the earth are shown in Fig. 1. The EOE position, which is 8.65 deg from the center of the earth for a synchronous orbit, is also shown.

As in the LES-6 system, the antenna system can be provided with a fail-safe mode of operation. Provisions are made for switching the antenna to yield an omnidirectional pattern in the event of failure in the sensing, logic, and switching circuitry. System gain would naturally be less (8 to 10 dB) than normal. However, certain communication links can still be provided between the satellite and the high-performance terminals.

B. SATELLITE AND ANTENNA MODEL

The RF performance characteristics of the antenna were evaluated with the use of a half-scale model. Figure 2 is a photograph of the satellite model with open-sleeve dipoles. The model is a right-circular cylinder of 42-in. diam and 38.7-in. height and is covered with a perforated aluminum sheet.

S1, S2 = BEAM SWITCHING POSITIONS
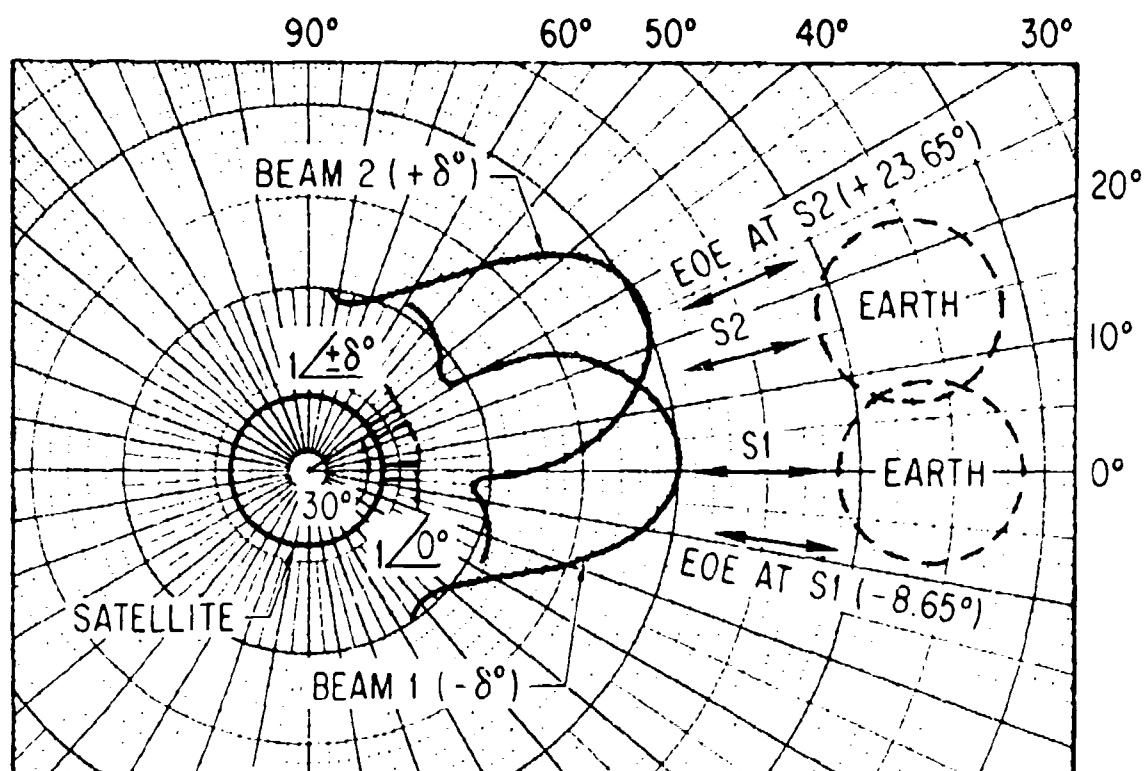
Figure 1. Antenna Beam and Switching Positions

Wideband impedance and pattern performance were obtained with open-sleeve dipoles (Refs. 3 and 4). A VSWR response of less than 2.5:1 was obtained over the 225 to 400 MHz band. Sleeve antennas generally have wider pattern bandwidth characteristics than conventional cylindrical (fat) dipoles (Ref. 5). In the present system, the dipoles and sleeves are of wire-grid construction for minimization of solar cell shadowing. The crossed, sleeve dipoles are shown in Figs. 2 and 3.

The original open-sleeve antenna reported by Barkley (Ref. 6) consisted of a dipole with two closely spaced parasitic elements. The length of the parasites (sleeves) was approximately one-half that of the center-fed dipole. An experimental study (Ref. 3) indicated that a wide variety of sleeve configurations can be used without any degradation in the VSWR response. For simplicity of construction, a flat sleeve arrangement was selected for this study. The flat wire-grid construction and the Styrofoam sleeve supports are shown in Figs. 2 and 3.

The construction details for the crossed, open-sleeve dipoles, dielectric supports, and balun are given in Fig. 4. The wire-grid assembly consists of 0.020-in. diam steel wires spot-welded together and subsequently silver plated. This construction simulates a solid metallic surface. The effective diameter (Ref. 7) of a wire-grid dipole can be expressed as

$$d_{eff} = d \left(\frac{n\, d_o}{d} \right)^{1/n}$$

where

   d = diameter of the wire "cage"

   n = number of wires

   d_o = diameter of wires
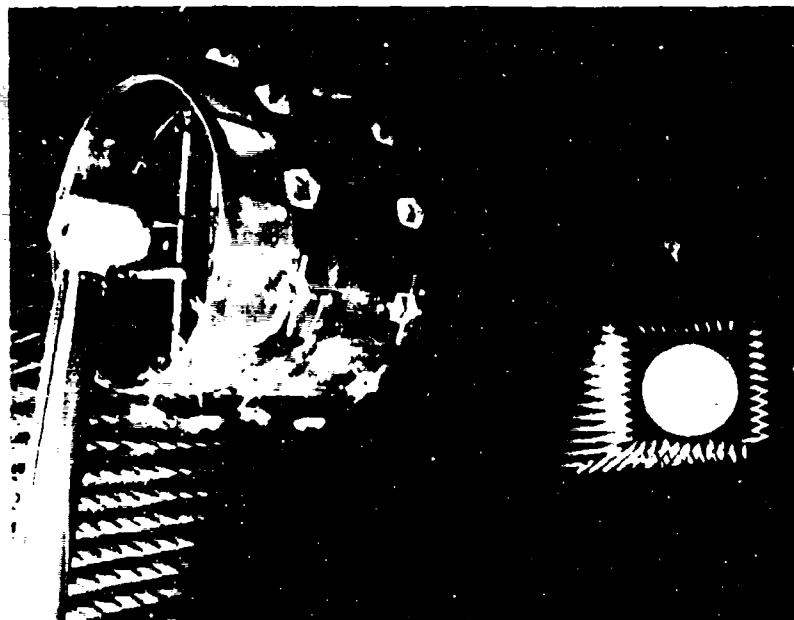
Figure 2. Photograph of Satellite Model With Open-
Sleeve Dipoles
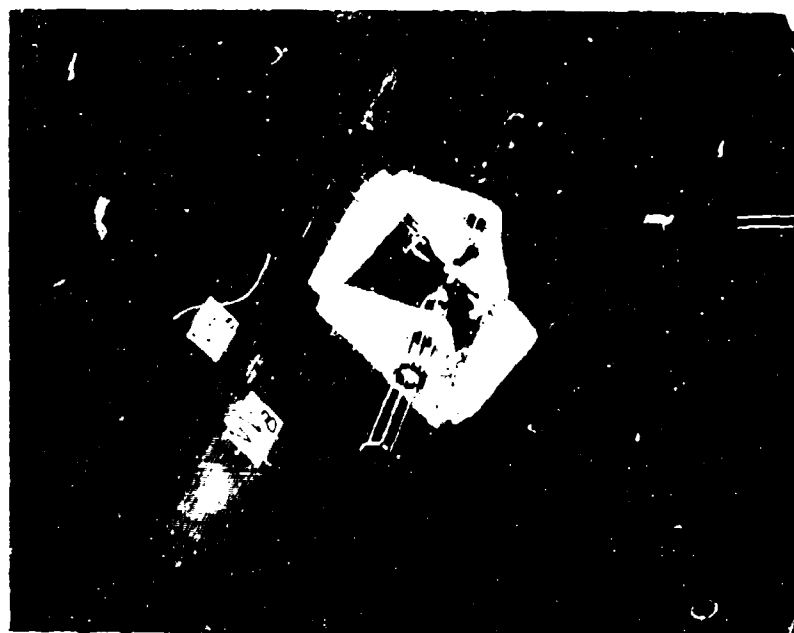
Figure 3. Closeup View of Crossed, Open-Sleeve
Dipoles

ALL DIMENSIONS
IN INCHES

0.141
SEMIRIGID COPPER
COAXIAL CABLE

FEED POINT DETAIL

0.413

0.250

DIRECT
CONNECTION

0.875

45°

0.150

2.5

0.030
WIRE, 0.50 CC

0.375

0.141

8 WIRES, 0.020
45° APART ON 0.563 B.C.

5.25

10.1

LONGITUDINAL WIRES
NOT SHOWN IN SIDE
VIEW OF DIPOLES

0.75

5

SATELLITE SURFACE
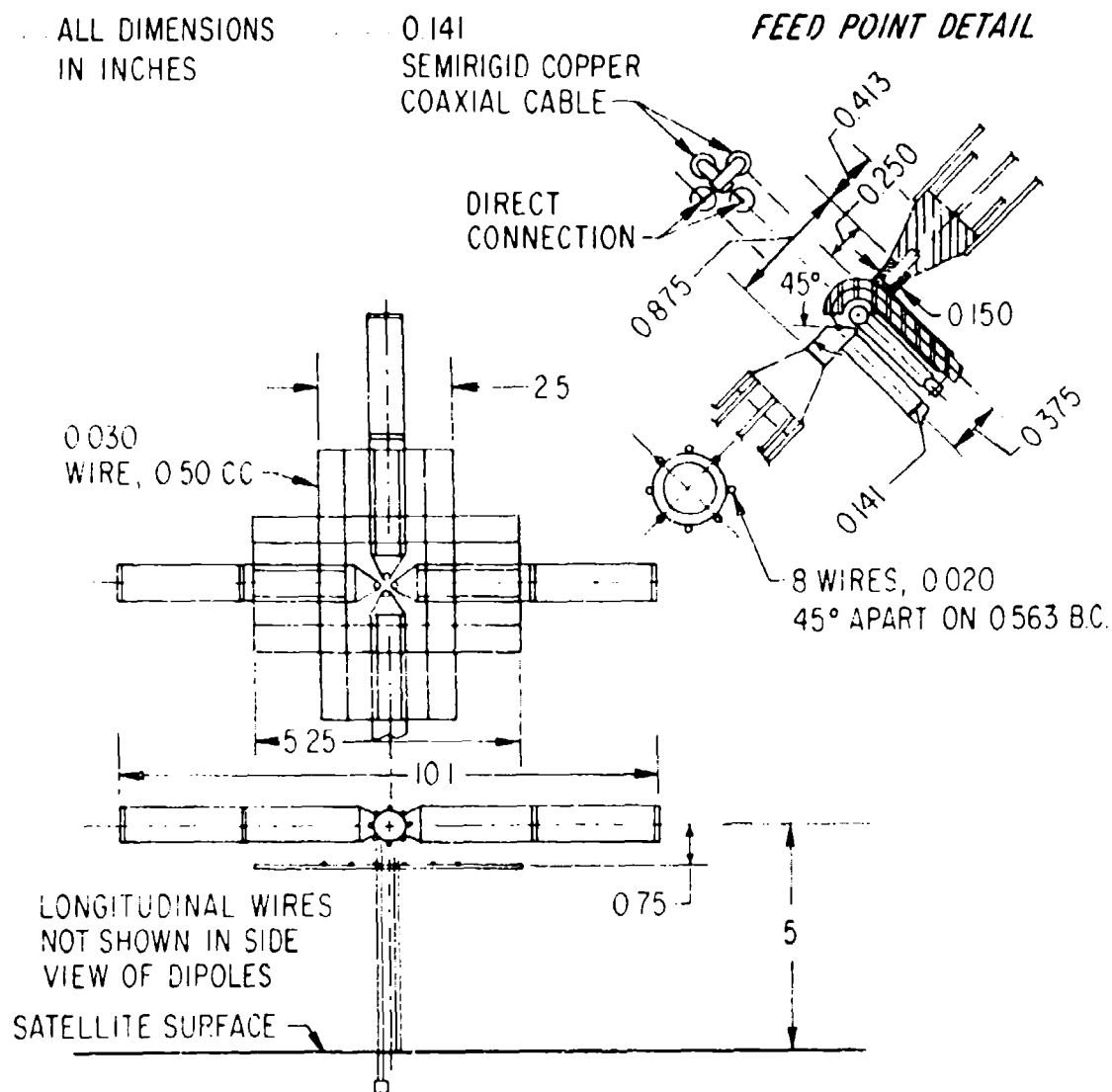
Figure 4. Half-Scale Model of Crossed, Open-Sleeve Dipoles

Thus, the effective diameter of the dipole shown in Fig. 4 is 0.481 in. The number of wires used in the flat sleeves was determined experimentally by noting the change in VSWR response when wires were added to or removed from the sleeves.

The feed line for the dipole (Fig. 4) is a copper-clad, 0.141-in. diam, semirigid coaxial cable. The balanced line of the balun is also a length of this semirigid cable but without the center conductor. The short circuit of this line is coincident with the reflector surface. The dipoles are screwed into the feed terminals, and the sleeves are supported by Styrofoam.

The polarizer unit used to achieve quadrature phase relations between the orthogonal dipoles consisted of a wideband hybrid (Anzac Electronics, Model No. II-8) and a 90-deg phasing cable cut for each of the test frequencies. (Wideband quadrature hybrids were not available for the experiments.) Four crossed dipoles (2 × 2 array) were fed simultaneously through a corporate feed structure as shown in Fig. 5. For reference, Fig. 5 also shows the relative positions of the antenna elements and the coordinate system used in the measurements.

The feed for each dipole is considered to be from the feed-input port to the dipole-balun port. The measured insertion loss characteristics are shown in Fig. 6. The data points represent the average loss as detected at the eight dipole-balun ports; the bars represent the peak deviation of the measurements. The true feed network insertion loss is defined as the measured power transfer less the 9 dB associated with the cascading of three 3-dB power dividers. The input VSWR to the feed network when the eight dipoles were connected according to Fig. 5 is shown in Table 2.

Table 2. Feed Network Input VSWR

Frequency, MHz	VSWR
450	1.15
500	1.26
600	1.20
700	1.25
800	1.36
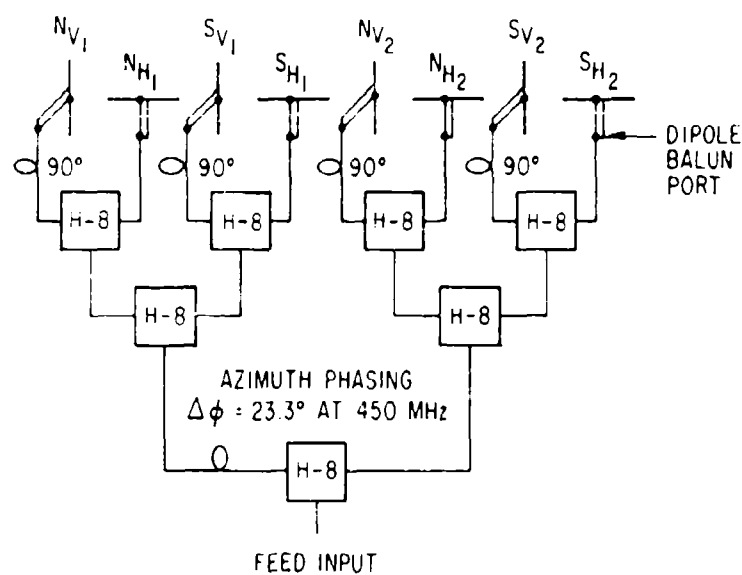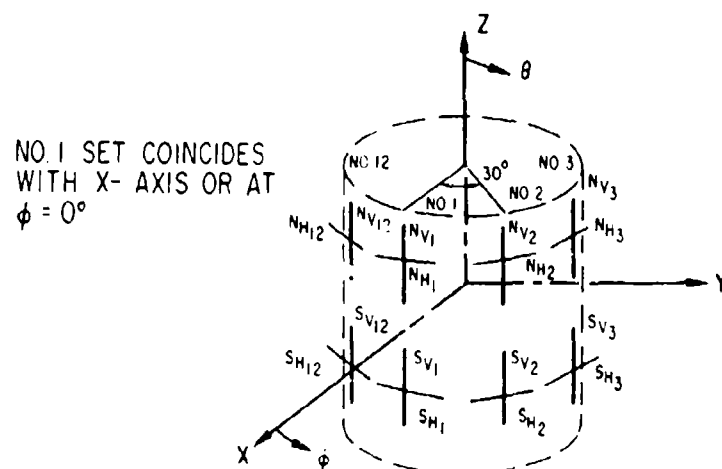
Figure 5.   Coordinate System and Antenna Feed Network

For most of the measurements, the axial spacing between the dipoles on the model was 20 in. (40 in. full-scale). Some data were also obtained with spacings of 18 and 22 in. Normally, the dipole-to-satellite spacing was 5 in. (10 in. full-scale). However, some measurements were also made with spacings ranging from 4.31 to 6.25 in. A length of RG-58/U cable was used to provide the phase delay, and a relative phase of 25 deg at 225 MHz was used between the elements in the azimuth ϕ plane.
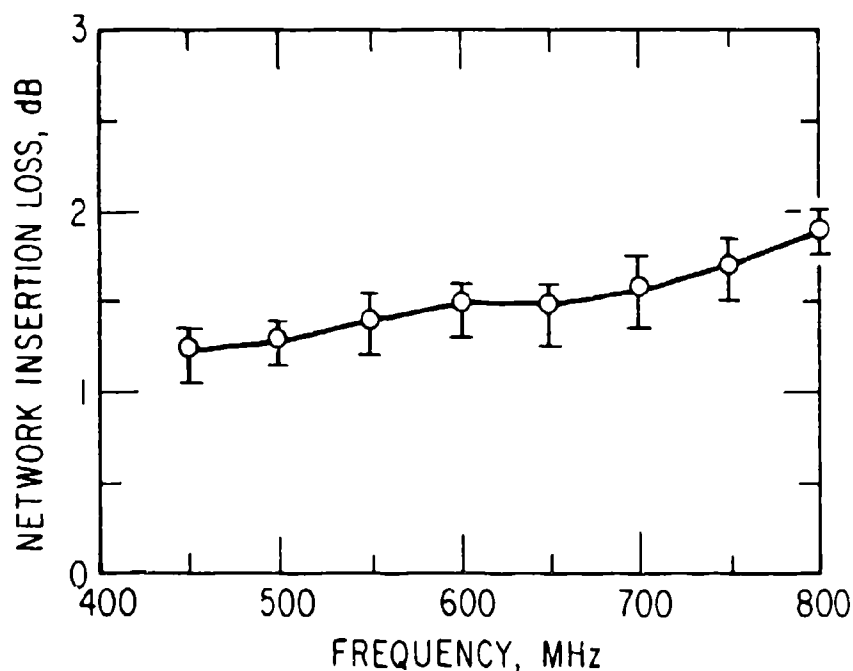
Figure 6. Insertion Loss of Antenna Feed Network

III. RESULTS

A. PATTERNS AND DIRECTIVITY

1. 20-IN. AXIAL DIPOLE SPACING AND 5-IN. DIPOLE-TO-REFLECTOR SPACING

The measured radiation patterns in the equatorial (azimuth) and polar (longitudinal) planes of the satellite are shown in Figs. 7 through 11. For these measurements, the axial spacing between dipoles was 20 in., the dipole-to-reflector spacing was 5 in., and the azimuth phasing cable was equivalent to 25 deg at 450 MHz.

The patterns were measured in an anechoic chamber (Ref. 8) with the transmitting antenna comprised of a 6-ft diam parabolic reflector located at the tapered portion of the chamber (Fig. 2). The parabola was illuminated with a conventional sleeve dipole (Ref. 5) feed mounted in a cylindrical cup (Ref. 9) such that the E and H plane patterns were equalized. The dipole was rotated at a speed of 60 to 80 rpm as the patterns were recorded. This provided a measure of the axial ratio of the test antenna at all aspect angles.

The response to a circularly polarized wave can be obtained from the pattern recordings by taking the RMS value of the maximum and minimum amplitudes (major and minor axis of the polarization ellipse) at each aspect angle. The half-power beamwidth (HPBW) of the patterns for a circularly polarized wave are shown in Fig. 12. The data points represent the average values of three to seven measured patterns; the bars represent the maximum deviation. The ϕ pattern shows an increase in the HPBW at 700 MHz. This is believed to be due to a "resonance" effect caused by the arrangement of the sleeves. This resonance effect would occur at other frequencies if other sleeve configurations were used.

Gain measurements were made on the half-scale model by using the substitution method. In this method, the satellite antenna is compared to a "standard gain" antenna, which is a corner reflector with a feed dipole tuned

-13-
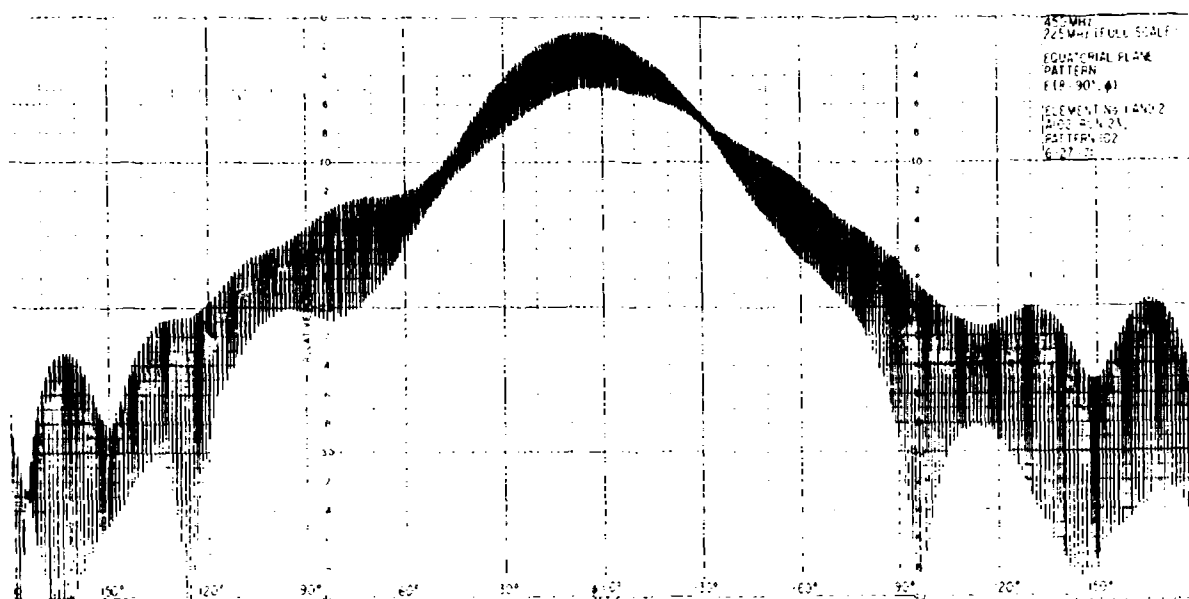
a. EQUATORIAL PLANE PATTERN
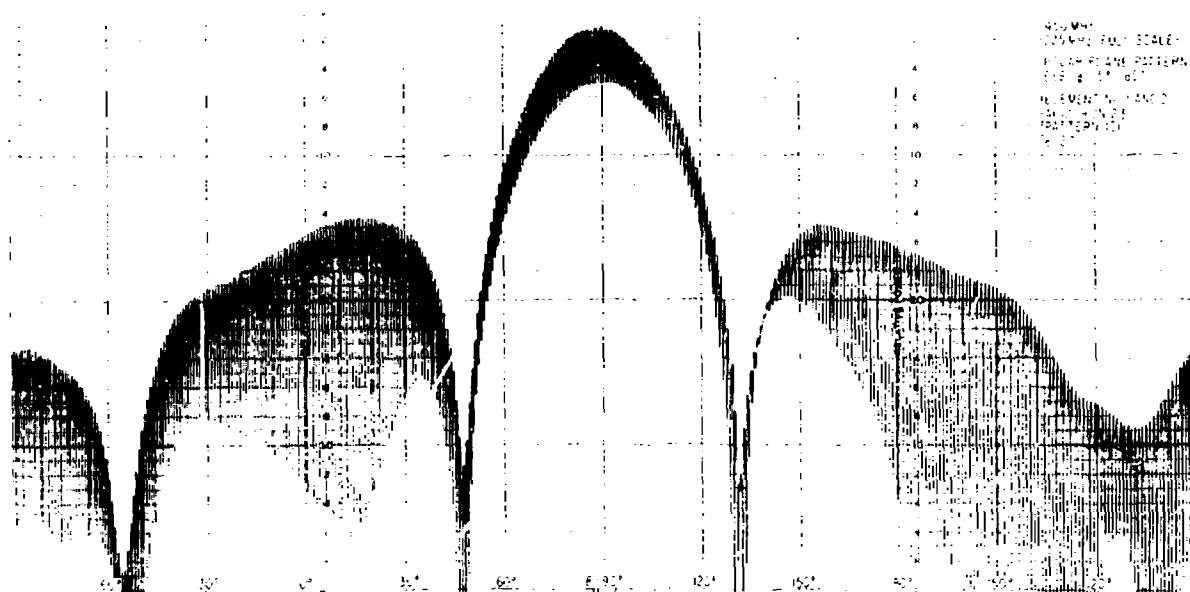
b. POLAR PLANE PATTERN

Figure 7. Measured Radiation Patterns of 2 × 2 Array at 450 MHz

-14-
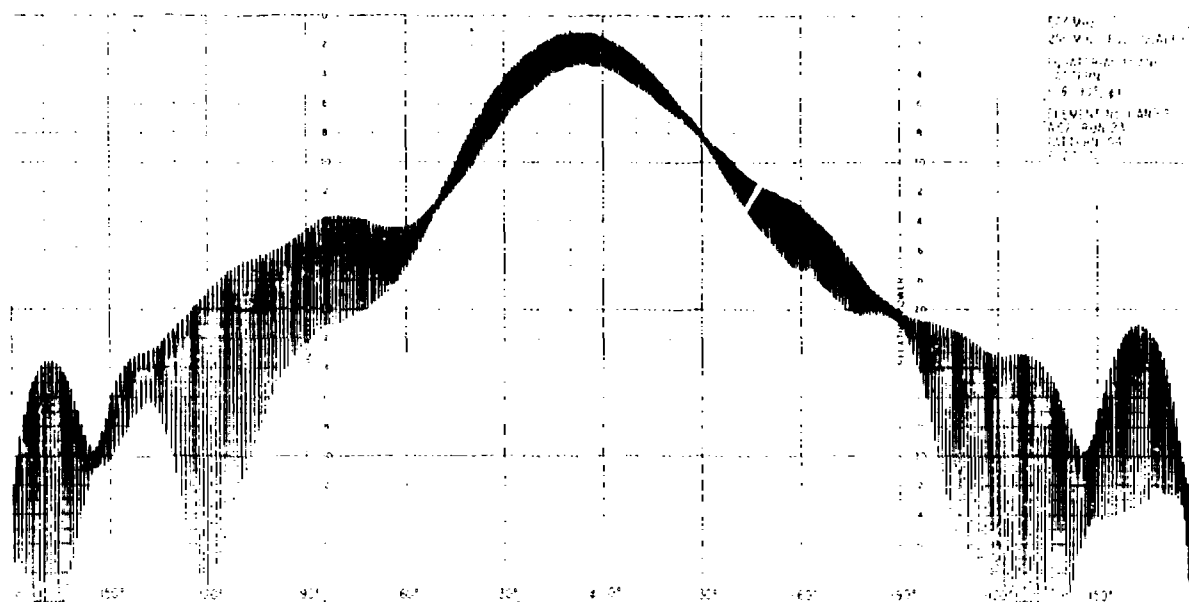
a. EQUATORIAL PLANE PATTERN
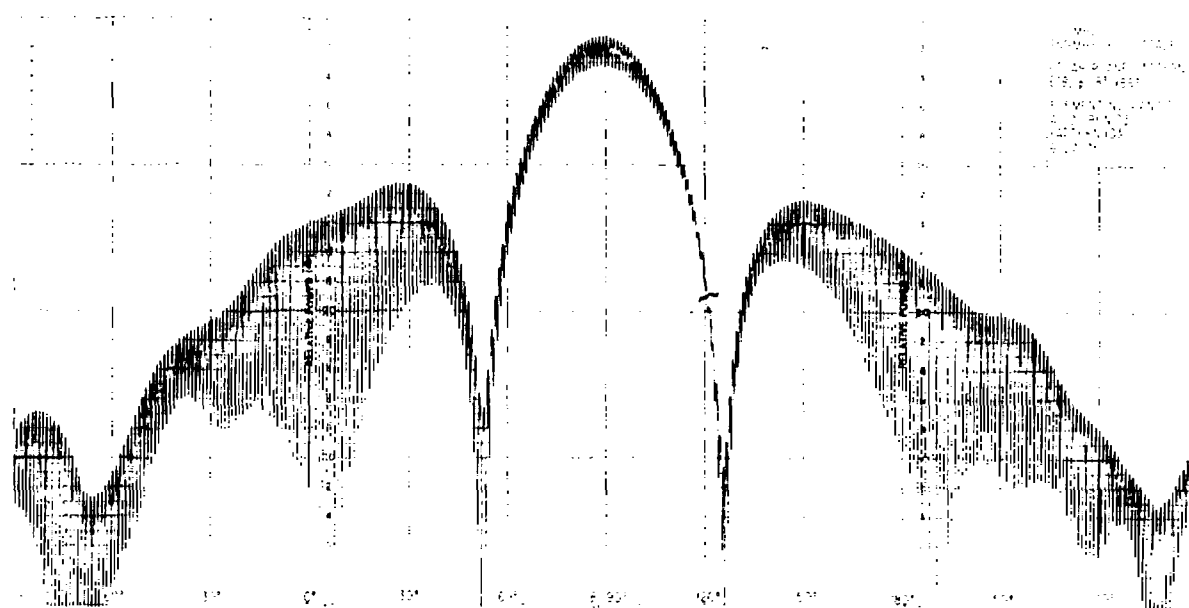
b. POLAR PLANE PATTERN

Figure 8.   Measured Radiation Patterns of 2 × 2 Array at 500 MHz
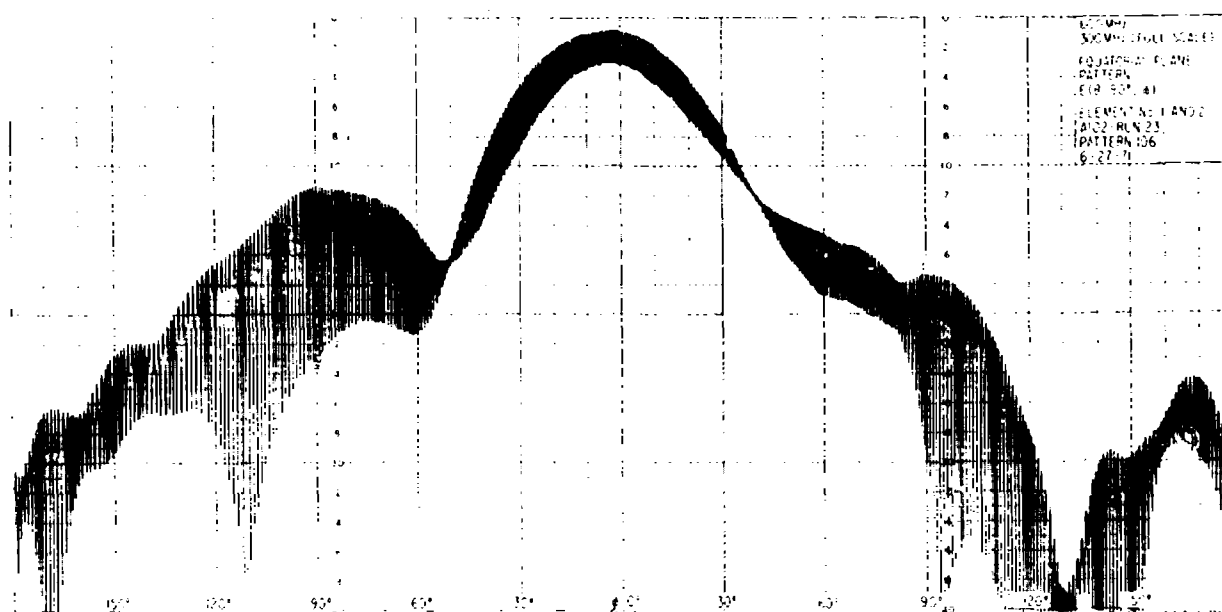
a. EQUATORIAL PLANE PATTERN
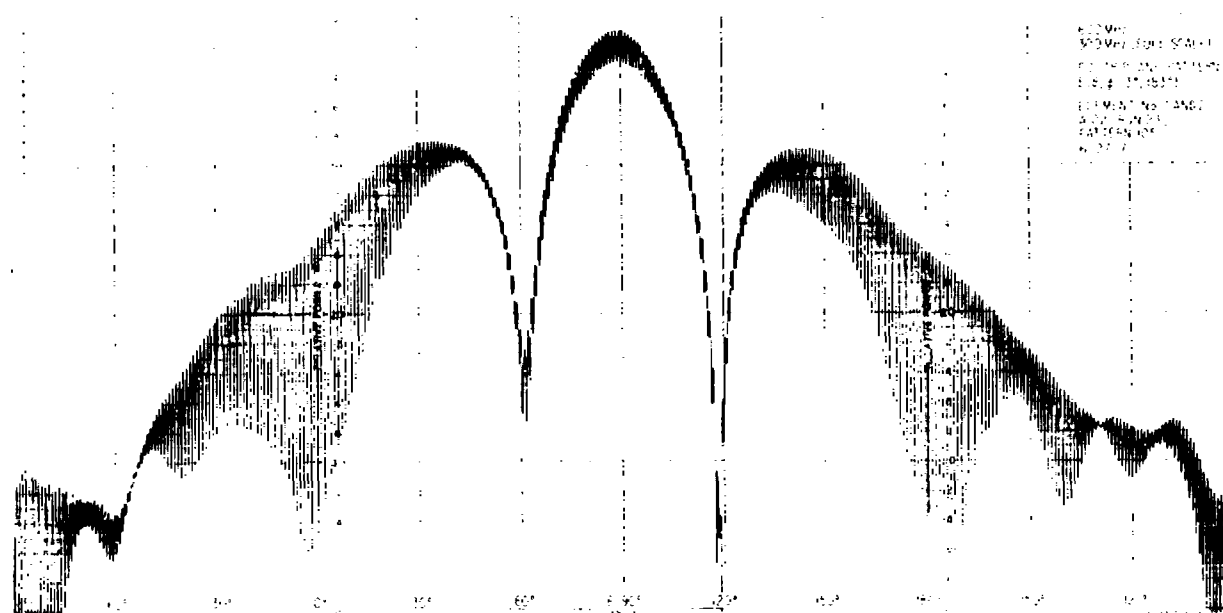
b. POLAR PLANE PATTERN

Figure 9.   Measured Radiation Patterns of 2 × 2 Array at 600 MHz

-16-
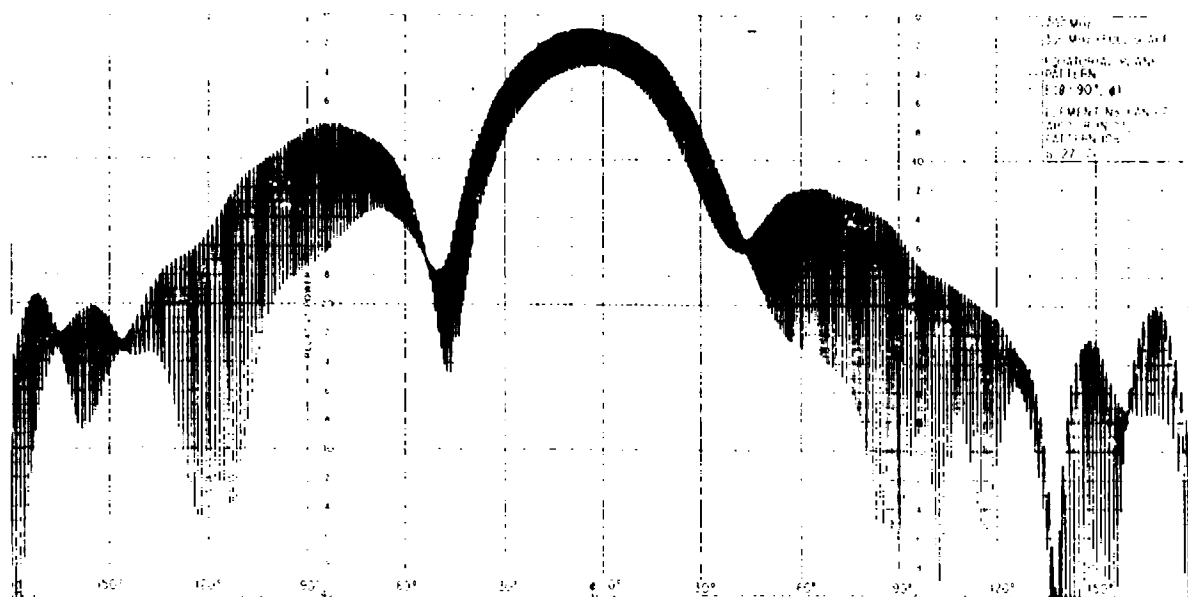
a. EQUATORIAL PLANE PATTERN
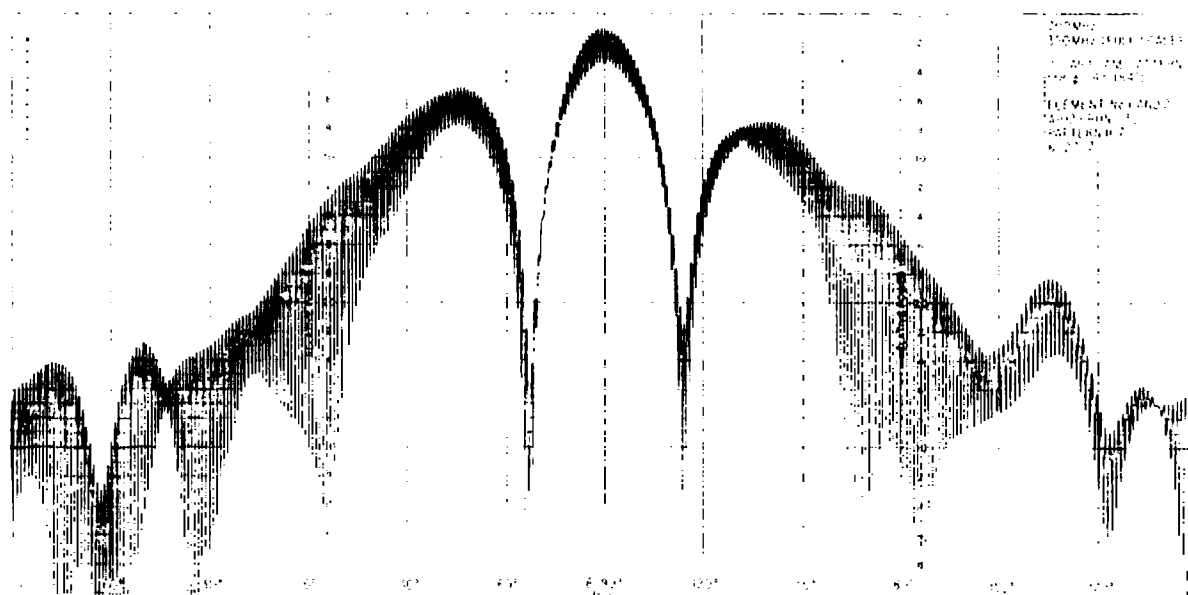
b. POLAR PLANE PATTERN

Figure 10.   Measured Radiation Patterns of 2 × 2 Array at 700 MHz

a. EQUATORIAL PLANE PATTERN

b. POLAR PLANE PATTERN

Figure 11. Measured Radiation Patterns of 2 × 2 Array at 800 MHz
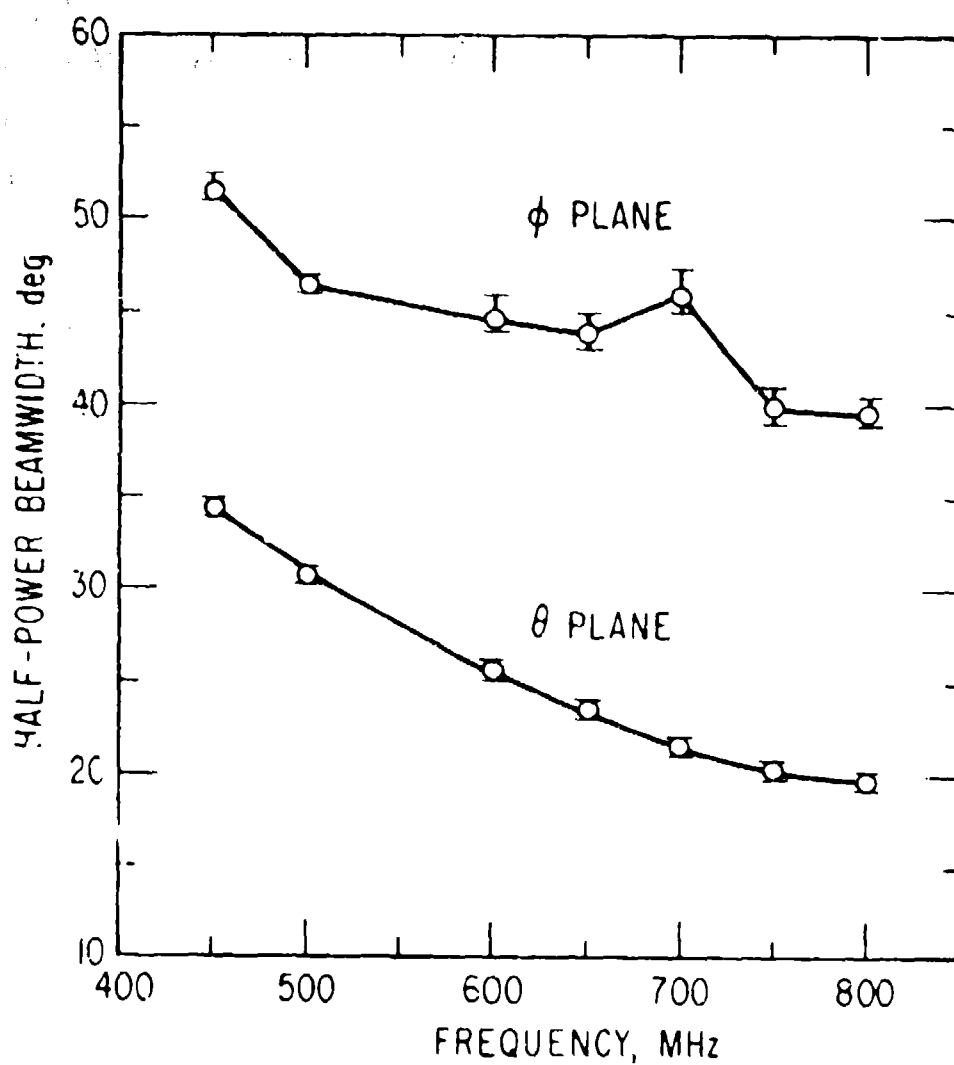
Figure 12. Measured Half-Power Beamwidths for a Dipole-to-Reflector Spacing of 5 in. and an Axial Spacing of 20 in.

for each of the test frequencies to yield a VSWR of less than 1.2:1. Two mechanically identical corner reflectors were made for each of the test frequencies and calibrated on an outdoor antenna range by using the two-antenna method. Measurements were obtained for several different distances between antennas. The standard deviation was less than 0.15 dB.

A typical corner reflector that was used as the reference antenna is shown in Fig. 13. For each gain measurement, the reference signal was recorded with the corner reflector mounted as shown in Fig. 14. The corner reflector was removed when the signal from the test antenna was being recorded. Care was taken to ensure that the phase center of the satellite antenna (assumed to be at the surface of the cylinder) and the corner reflector were located the same distance from the transmitting antenna.

At each test frequency, the gain was measured at three different range distances, at two satellite positions (+Z axis pointing to the east and then to the west), and with the transmitting antenna polarization aligned along the major axis of the polarization ellipse. This procedure was repeated with the polarization aligned with the minor axis of the polarization ellipse. Thus, each data point for a given frequency represented the average of 12 measurements. Correction factors were used to normalize the gain of the satellite antenna with respect to a circularly polarized wave source since linearly polarized transmitting and reference antennas were used. Independent gain measurements were made as the experimental program proceeded in order to obtain a good estimate of the mean gain and its variance. These measurements were made under the following conditions: (1) with cables disconnected, then reconnected, (2) with other groups of dipoles, and (3) with both of the calibrated reference antennas. These different conditions together with repeated measurements provided sufficient data for determination of a mean value for the gain.

The results of the array gain measurements are shown in Fig. 15. The data points (circles) represent the mean values for each frequency, the
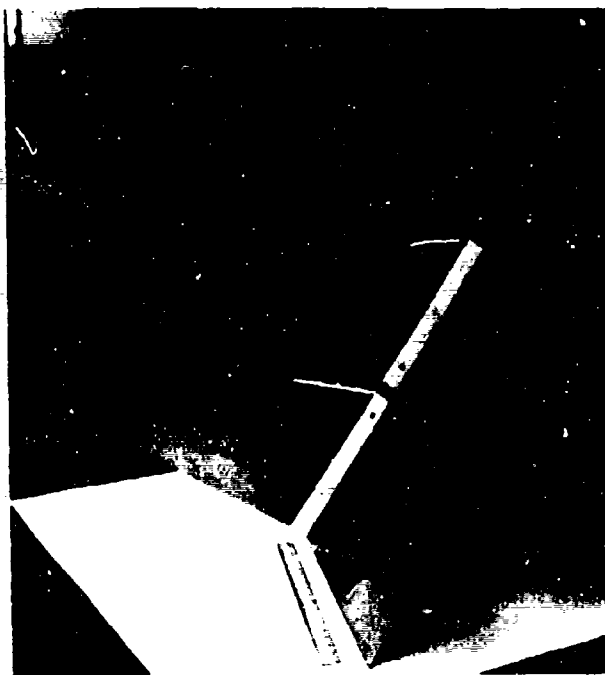
Figure 13. Corner Reflector Used as a
Reference Standard Gain
Antenna

Figure 14. Corner Reflector Mounting
Arrangement for Gain
Measurements
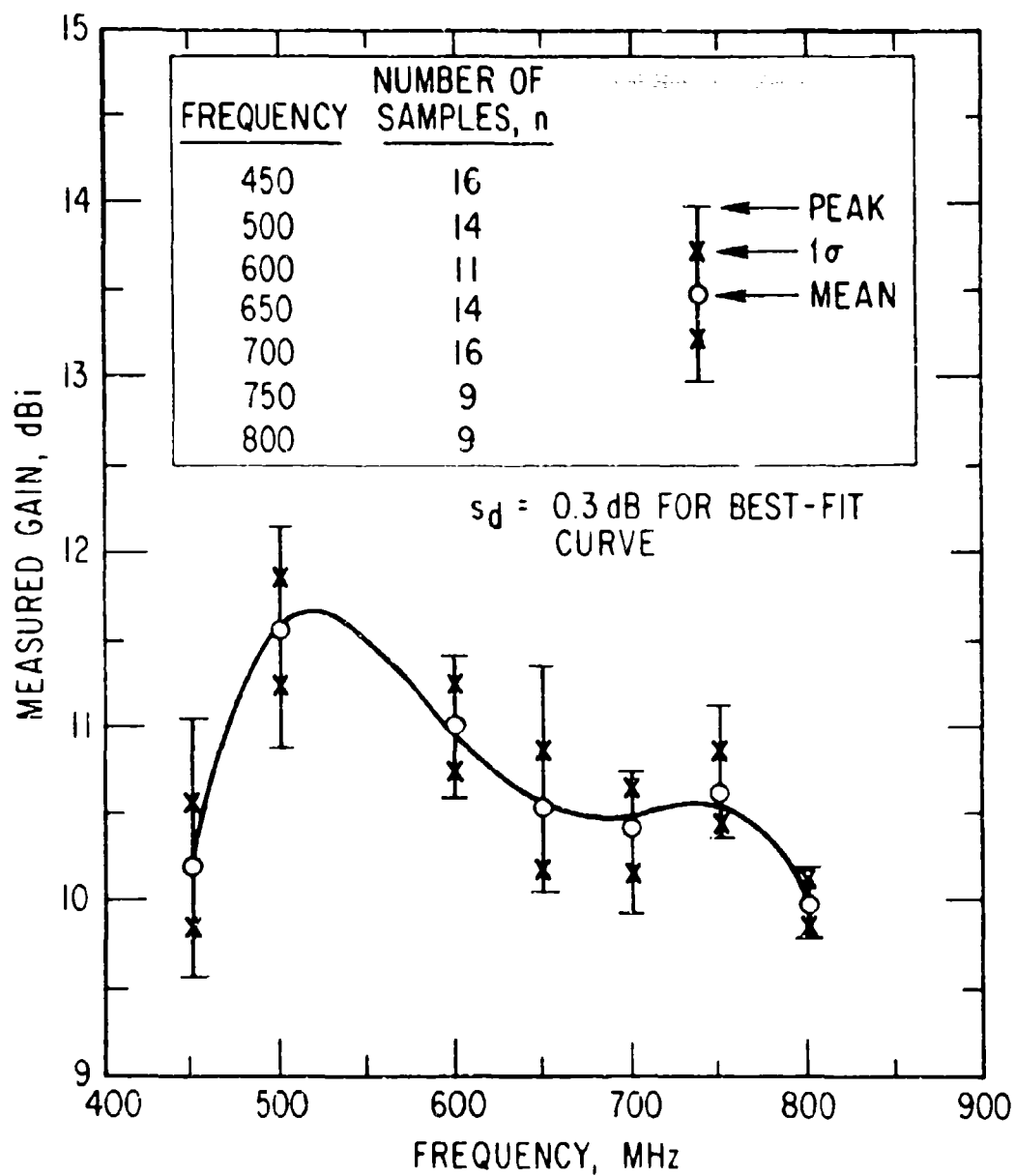
Figure 15. Measured Gain of Array Referenced to Feed Network Input

-22-

bars represent the scatter of the data, and X represents the standard deviation s_d. The curve is a fourth-order polynomial equation least squares fit to the data. The standard deviation of the best-fit curve is 0.3 dB; n indicates the number of samples used.

The measured directivity was determined by adding the feed network loss, which is the loss from the feed input to the balun terminal, and the mismatch loss to the measured gain. The network loss is shown in Fig. 6. The mismatch loss was determined from the VSWR of an individual dipole looking into the balun terminals (Section IIIB). The measured directivity is shown in Fig. 16. The RSS value of the variances, i.e., reference antenna calibration (0.2 dB, 1σ), feed network losses (0.1 dB, 1σ), mismatch losses (0.1 dB, 1σ), and the array gain measurements, was used to obtain a value of 0.39 dB for the overall deviation of the measured directivity.

The directivity was also obtained by numerical integration of the measured radiation patterns over 4π sterad. "Conical cuts," i.e., patterns defined by $E(\theta = \theta_1, \varphi)$, were made in 5-deg increments of θ to obtain the volumetric radiation pattern of the array. The directivity can be calculated from

$$D = \frac{4\pi}{\int_0^{2\pi}\int_0^{\pi} E^2(\theta, \varphi)\sin\theta \, d\theta \, d\varphi} \tag{1}$$

The antenna directivity computed by graphical integration of a set of radiation patterns is shown in Fig. 17.

The difference between the measured and computed directivity is considered to be the loss in the antenna element. This loss can be attributed to the dipole, sleeves, balun, reflector, and other unaccountable factors. On the average, the antenna loss is 0.28 dB.

The computation of directivity by graphical integration of the measured radiation patterns is a time-consuming task. It requires approximately 8 hr

-23-
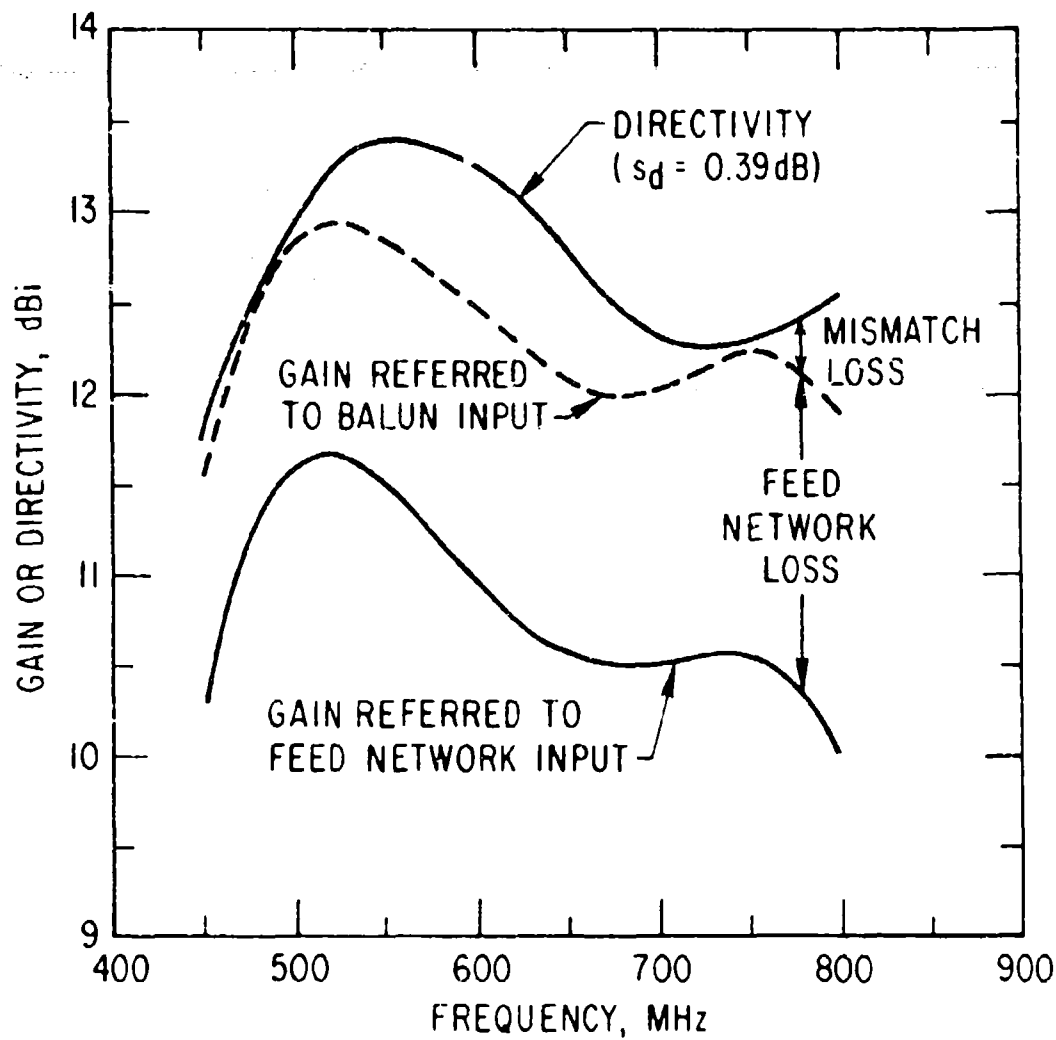
Figure 16. Measured Directivity of Array
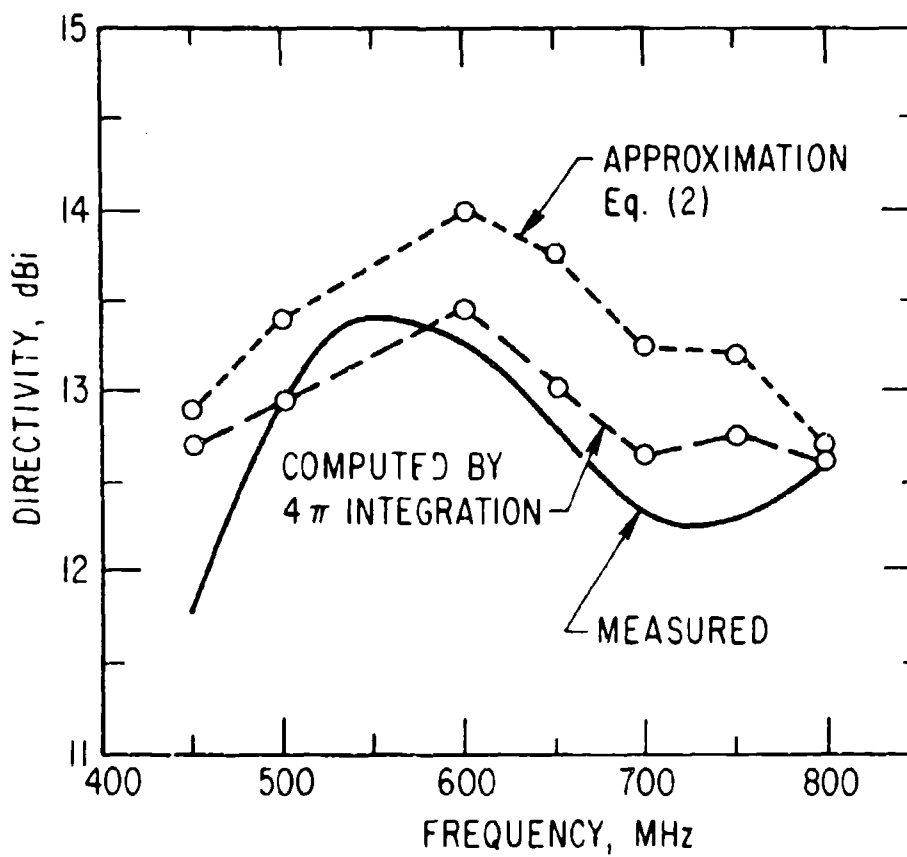
Figure 17. Directivity Determined From Integration of the Measured Radiation Patterns

of pattern measurements in addition to the time required for data reduction. Therefore, a more simplified procedure for obtaining a rapid estimate of the directivity is desirable. A reasonable approach is the use of the patterns in the two principal planes, i.e., $E(\theta, \phi = \phi_1)$ and $E(\theta = 90°, \phi)$, where ϕ_1 is the angle of maximum intensity in the equatorial plane. The antenna directivity can be approximated (Ref. 4) by

$$D = D_V D_H \tag{2}$$

where

$$D_V = \frac{2}{\int_0^\pi E^2(\theta, \phi = \phi_1)\sin\theta\, d\theta} \tag{3}$$

and

$$D_H = \frac{2\pi}{\int_0^{2\pi} E^2(\theta = 90°, \phi)d\phi} \tag{4}$$

where the pattern is normalized to the beam peak. D_V is the directivity enhancement in the "vertical" plane pattern as if the azimuthal pattern were omnidirectional, and D_H is the enhanced directivity in the "horizontal" plane since the array pattern is not omnidirectional. This approximation is based on the assumption that the θ plane patterns are independent of the angle ϕ and vice versa. Experimental data have indicated that the relative shape of the θ plane patterns are fairly close for various angles of ϕ in the major portion of the main beam, i.e., $E(\theta, \phi = \phi_1) \approx C\, E(\theta, \phi = \phi_2)$, where C is a constant, and ϕ_1 and ϕ_2 are confined to within 10 dB of the main beam peak.

The directivity as compared with the integration of the measured patterns over 4π sterad is shown in Fig. 17 based on the approximation of Eq. (2).

The comparison is within 0.75 dB and averages 0.44 dB. The $D_V D_H$ values for each frequency were derived from the integration of a number of patterns (a minimum of four). The average standard deviation of all the mean values is 0.2 dB; the highest is 0.36 dB. This procedure yields fairly accurate results for rapid estimation of the directivity. In many cases, only the principal plane patterns are available.

The EOE gain is the important factor for the systems engineer in determining the power budget. In the polar plane, the decrease in antenna gain 8.65 deg from the beam peak is considered. In the equatorial plane, the EOE is considered to be 8.65 deg away from the two beam switching positions (Fig. 1), i.e., $\phi = -8.65$ and $+23.65$ deg. The measured EOE correction (decrease in gain from the beam peak) values for the two planes are shown in Fig. 18. The vertical bars represent the scatter of the data. The mean value for each frequency is also shown. A second-order least-squares fit curve is plotted, and the standard deviation from the best-fit curve is shown in each plot. For comparison, the theoretical EOE ripple is shown as the solid curve. The EOE directivities derived from the measured directivity and the experimental EOE ripple are plotted in Fig. 19. The standard deviation of the best estimate of the EOE directivities is noted on each curve. This was obtained by taking the RSS value of the standard deviation of both the measured directivity and the EOE ripple.

2. OTHER DIPOLE SPACINGS

In this section, the performance of the array is described for dipole-to-reflector spacings of 5.5 and 6 in. and an axial spacing of 20 in., and for a dipole-to-reflector spacing of 5 in. and axial spacings of 18 and 22 in. The pertinent pattern and gain characteristics with respect to a circularly polarized source are presented.

The radiation pattern characteristics for dipole-to-reflector spacings of 5.5 and 6 in. and an axial spacing between dipole elements of 20 in. are
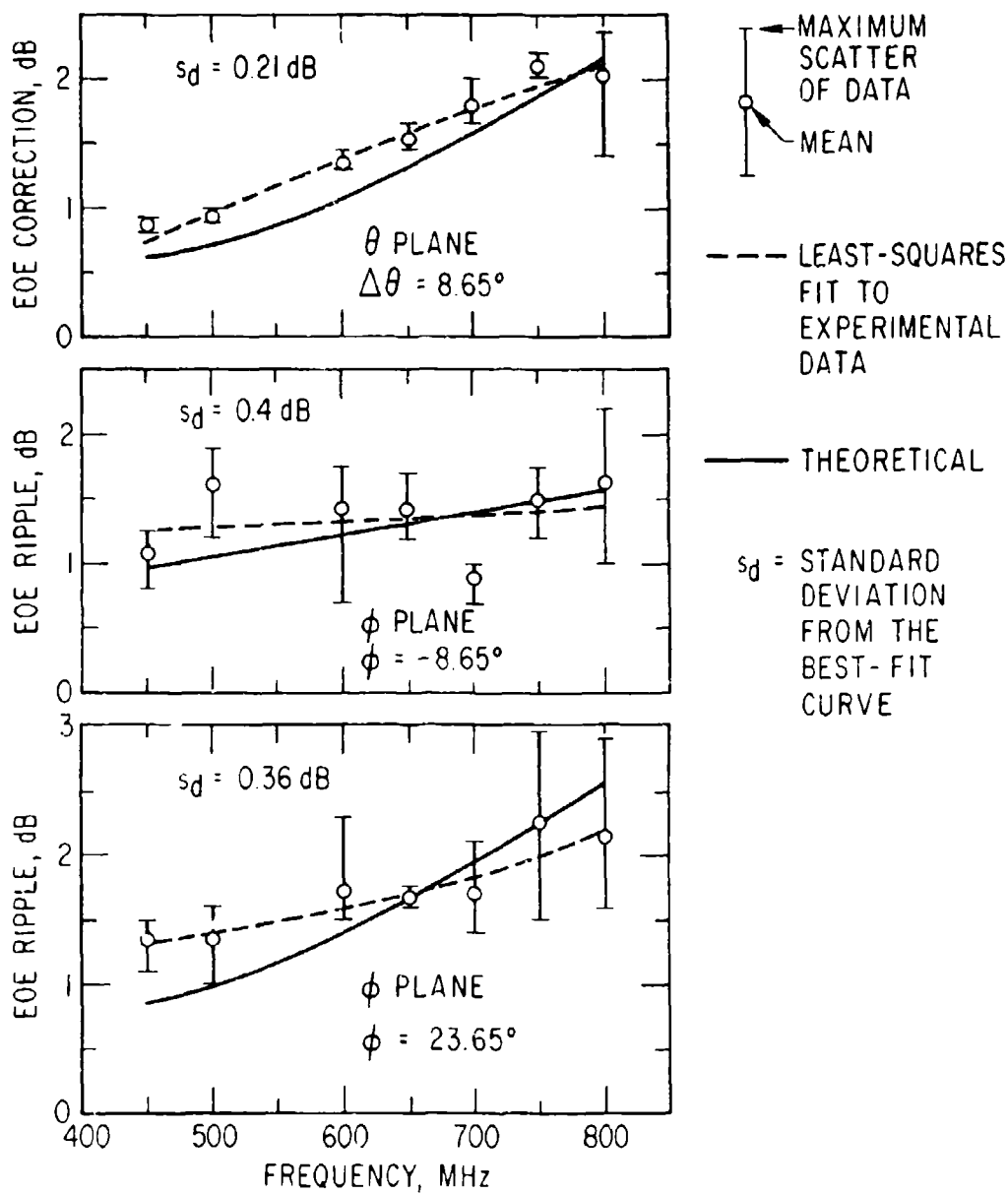
Figure 18. Measured and Computed EOE Correction for Equatorial
and Polar Planes for a Dipole-to-Reflector Spacing of
5 in. and an Axial Spacing of 20 in.
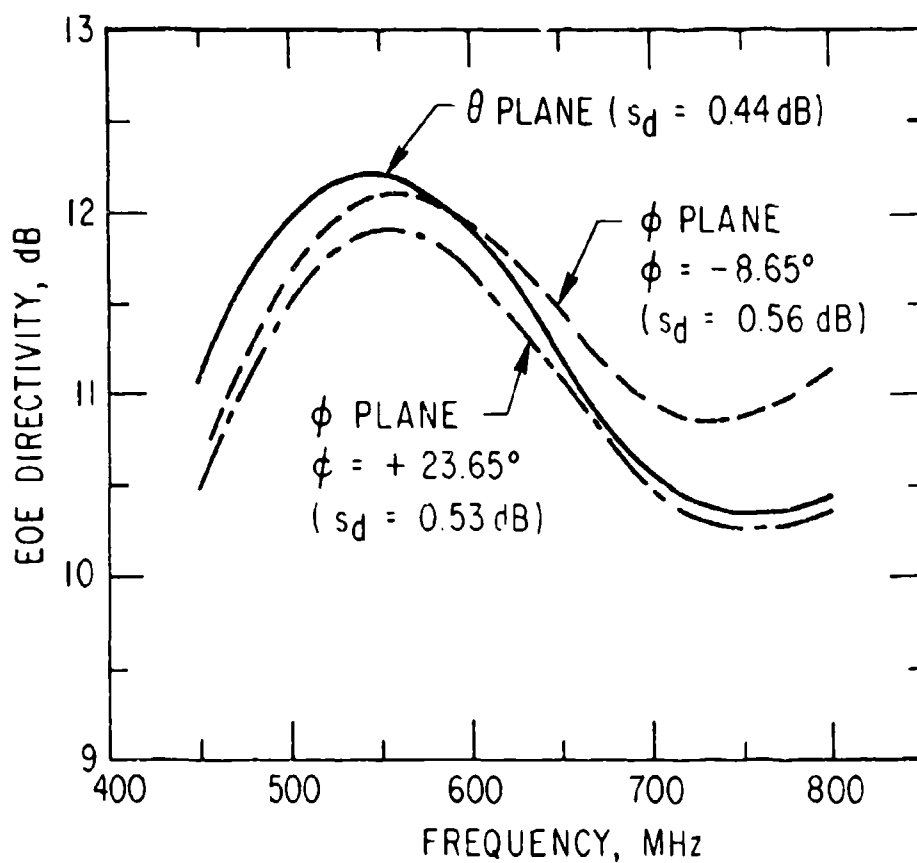
Figure 19. EOE Directivities Derived From the Measured
Directivity and the Experimental EOE Cor-
rection for a Dipole-to-Reflector Spacing
of 5 in. and an Axial Spacing of 20 in.

shown in Figs. 20 through 22. The measured patterns in the polar and equatorial planes are shown in Figs. 20 and 21, respectively. The half-power beamwidths are shown in Fig. 22. For comparison, the pattern characteristics for a dipole-to-reflector spacing of 5 in. are also shown.

Larger dipole-to-reflector spacings were also investigated for improvement in the VSWR of the dipole elements. The element pattern beamwidth is wider because the dipole-to-reflector spacing is larger than 0.25λ, which is the point where beam bifurcation begins to occur. An improvement in the VSWR was obtained (Section IIIB), but no significant change was observed in the gain and beamwidth characteristics at the low end of the frequency band. The beamwidth increased slightly at the high frequency end, thus decreasing the EOE ripple. However, this was offset by the decrease in directivity that was caused by the increased sidelobe levels. The measured directivities are shown in Fig. 23.

Figures 20 through 23 show that there are no significant changes in pattern and directivity characteristics at the low end of the frequency band because the element pattern beam bifurcation is not prominent. However, at the higher frequencies, where the dipole-to-reflector spacings are 0.37λ (5.5 in.) and 0.41λ (6 in.) at 800 MHz, a noticeable split is shown in the element patterns (Ref. 10). This causes a wider array beamwidth and increases the sidelobe levels. The sidelobe level change is shown in the patterns for both the polar and equatorial planes at 800 MHz. At 450 and 600 MHz, only the spacing patterns at 6 in. were plotted for comparison with those at 5 in. It should be noted that the excessive loss in gain was predominantly due to the increased sidelobe levels rather than the increased half-power beamwidths.

The measured half-power beamwidths for axial spacings of 18 and 22 in. and a dipole-to-reflector spacing of 5 in. are shown in Fig. 24. With a change in the axial spacing, only minor perturbations would be expected in the ϕ plane pattern. However, the θ plane would be expected to show the measurable pattern changes. The predicted gain change is only a few tenths dB from the nominal 20 in. spacing as illustrated in Fig. 25, which is a plot
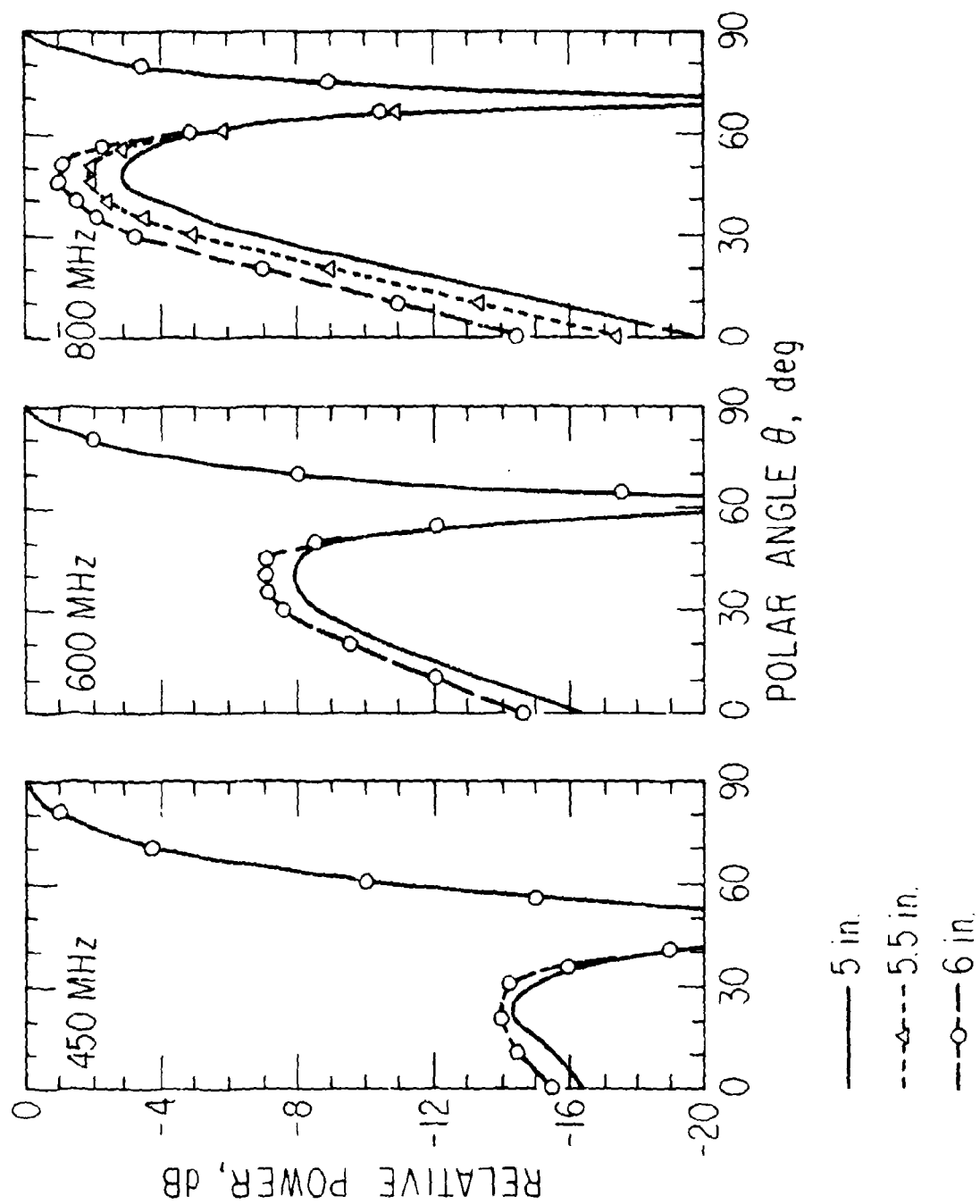
Figure 20. Measured Polar Plane Patterns for Dipole-to-Reflector Spacings of 5, 5.5, and 6 in. and an Axial Spacing of 20 in.
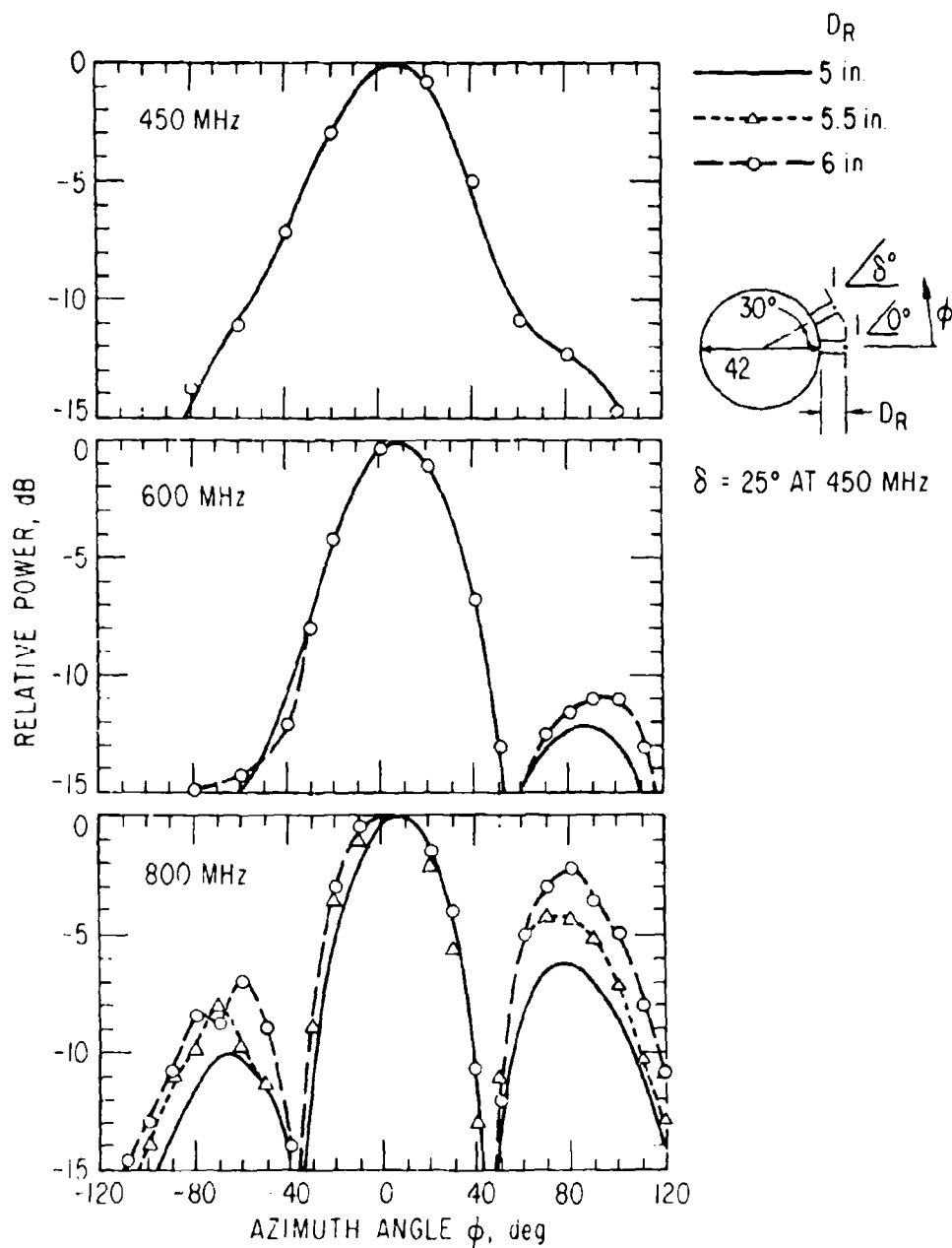
Figure 21. Measured Equatorial Plane Patterns for Dipole-to-Reflector Spacings of 5, 5.5, and 6 in. and an Axial Spacing of 20 in.
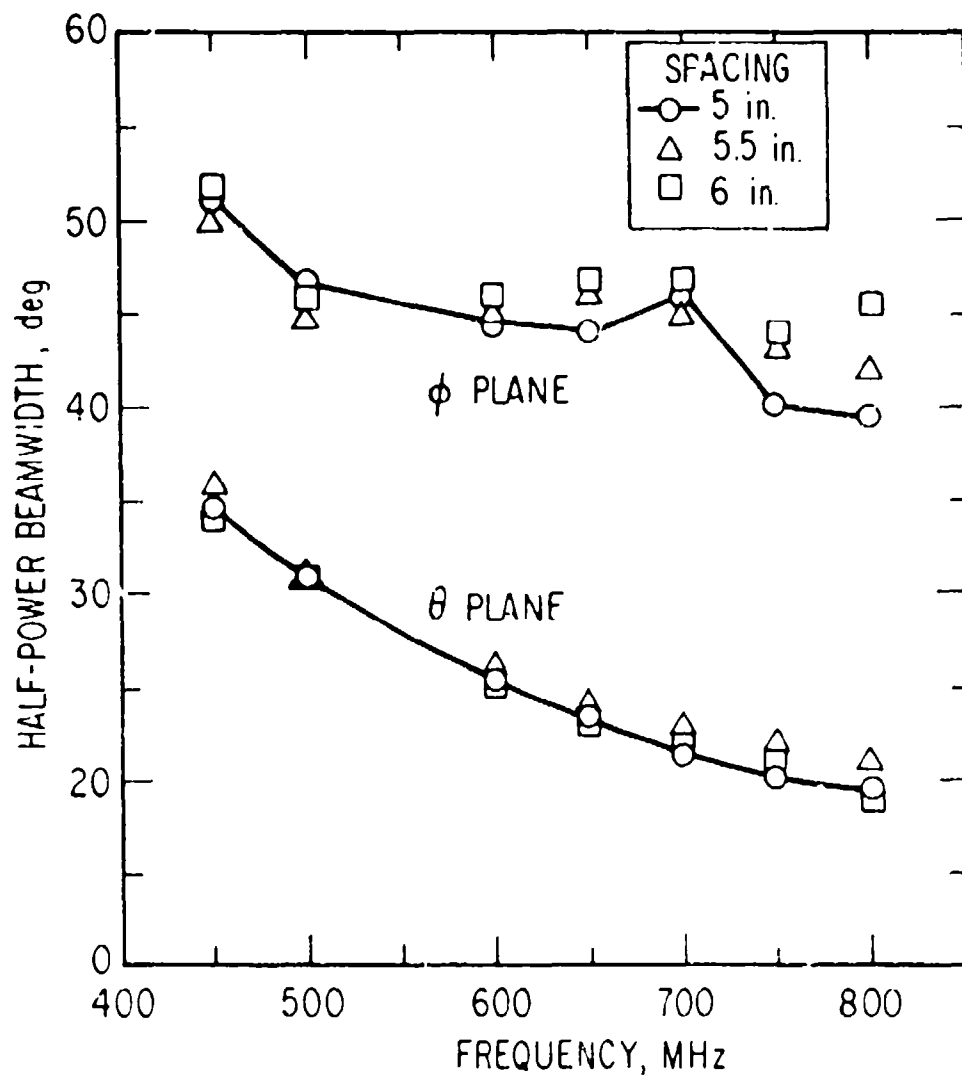
Figure 22. Measured Half-Power Beamwidths and Sidelobe
Levels for Dipole-to-Reflector Spacings of 5 to
6 in. and an Axial Spacing of 20 in.
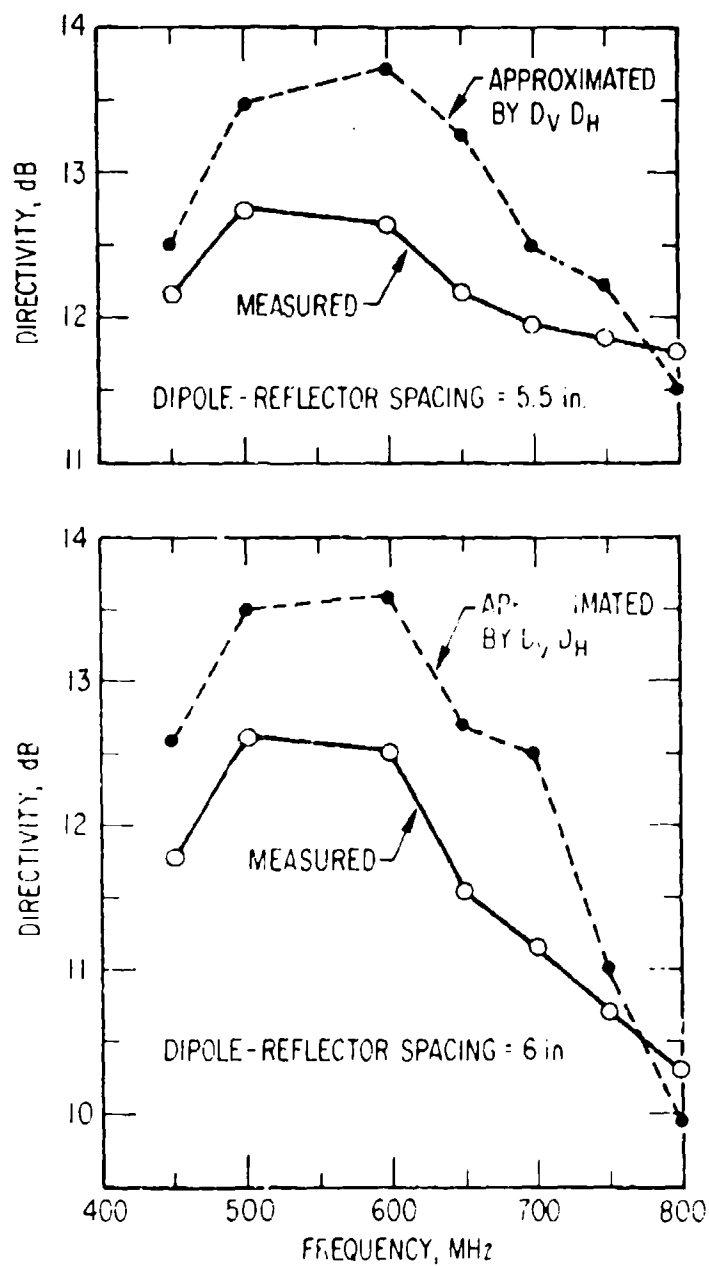
Figure 23. Measured Directivities for Dipole-to-Reflector Spacings of 5.5 and 6 in. and an Axial Spacing of 20 in.
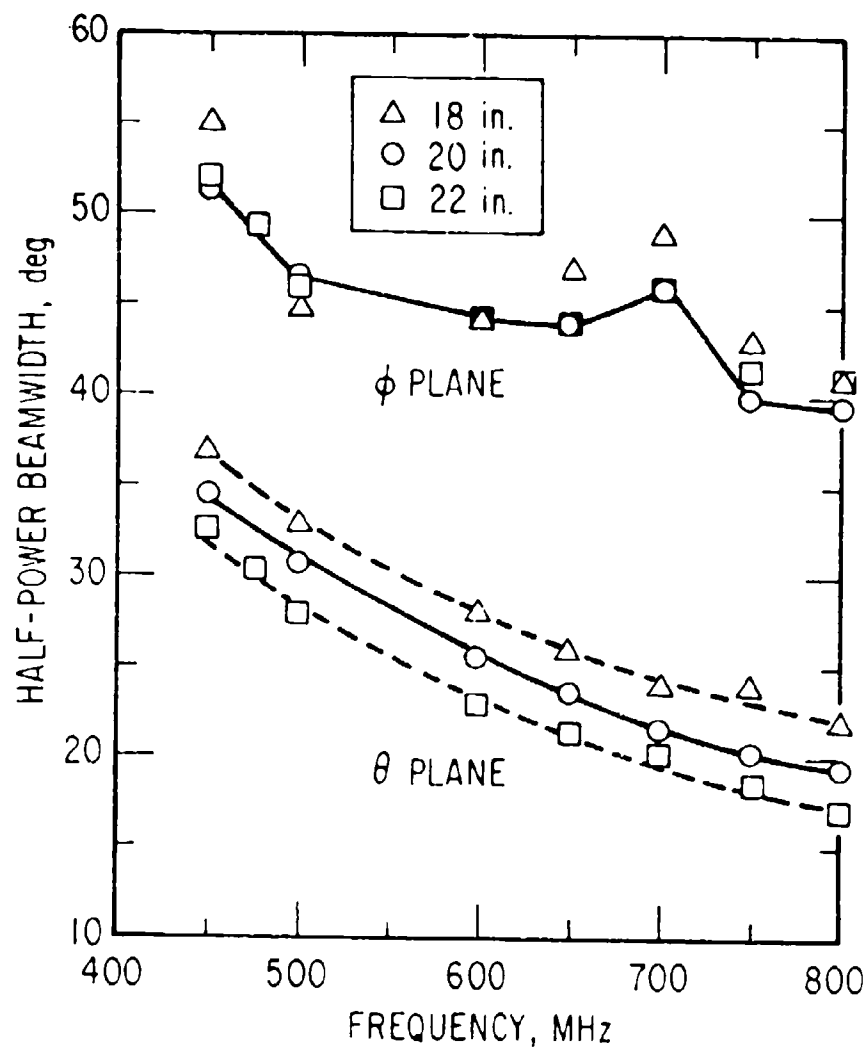
Figure 24.   Measured Half-Power Beamwidths for a Dopole-
to-Reflector Spacing of 5 in. and Axial Spacings
of 18 and 22 in.
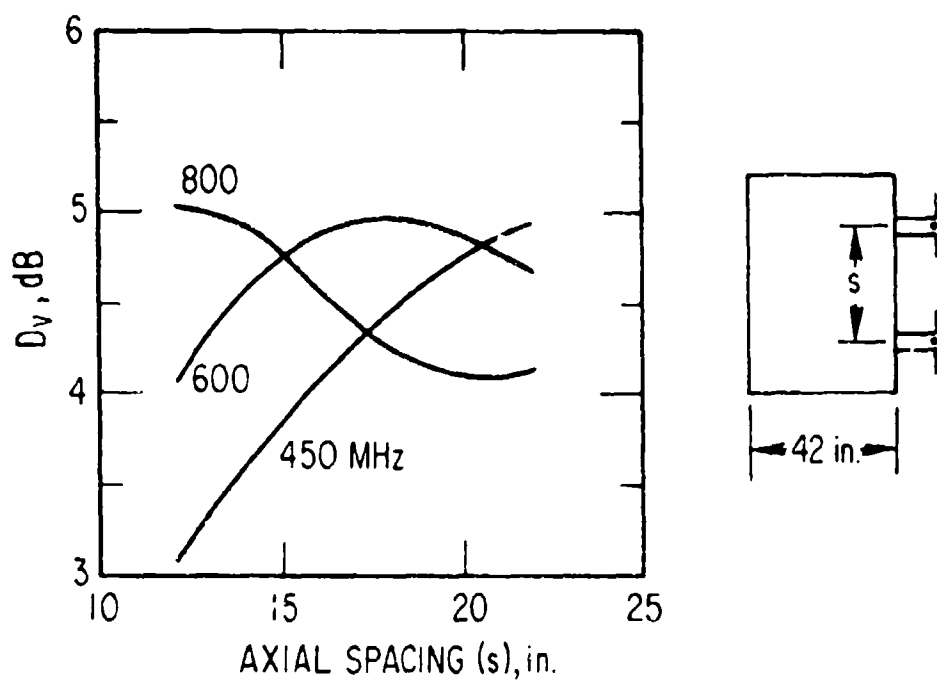
Figure 25.   Polar Plane Directivity Enhancement as a Function
of Spacing

of D_V as a function of the axial spacing, where D_V is the directivity enhancement in the θ plane. D_V was computed from Eq. (3) with the use of the measured element patterns (Section IIIA3). Because of the variance in the gain measurements, the chance of detecting a change of ± 0.25 dB with any significant degree of confidence would require many measurements. Therefore, gain measurements were not attempted. However, the differential gain can be established experimentally by determining D_V from the integration of the measured radiation patterns. In Table 3, the ΔD_V values as determined from Fig. 25 are compared with those from the measured D_V values.

Table 3. Comparison of Computed and Measured ΔD_V for Axial Spacings of 18 and 22 in.

Frequency, MHz	Measured D_V, dB		ΔD_V, dB	
	18 in.	22 in.	Measured	Computed
450	4.98	5.45	+ 0.47	+ 0.47
600	5.65	5.3	- 0.35	- 0.29
800	4.85	4.9	+ 0.05	- 0.12

3. COMPARISON OF MEASURED AND COMPUTED DATA

Patterns in equatorial and polar planes of the satellite were computed from a simplified array theory by using the measured element patterns of the wire-grid, flat-sleeve, crossed dipoles. In this section, comparisons are made of the measured and computed patterns, EOE ripple, and directivities. The element patterns were measured with the use of a right-circular cylinder of 30-in. diam and 48-in. height instead of the 42-in. diam satellite model because of a time and scheduling problem in the antenna laboratory. The cylinder, which was available from previous experiments, was covered with 1-in. wire mesh netting in order to simulate the metallic surface of the satellite. For the intended objectives of the study, the differences in the element pattern measured on a 42-in. and a 30-in. diam model were not expected to significantly affect the results of the array computations.

-37-

The crossed, open-sleeve dipoles (Fig. 3) were mounted midway along the surface of the cylinder and spaced 5 in. from the metal surface. E and H plane patterns were recorded for both the axially and transversely mounted dipoles. The response for circular polarization was derived by calculation of the RSS value of the two measured field components. For example, the RSS field in the azimuth plane is given by $\sqrt{E_1^2 + E_2^2}$, where E_1 is the H-plane pattern of the axial dipole, and E_2 is the E-plane pattern of the transverse dipole. The polar plane pattern was determined in a similar manner. The element patterns of the crossed dipoles in the azimuth and polar planes are shown in Figs. 26 and 27, respectively. It is interesting to note that the element patterns can be closely approximated by

$$E_e(\varphi) = 0.224 + 0.776 \cos^{1.475} 0.75\varphi \quad , \qquad 0 \le |\varphi| \le 120°$$

$$E_e(\theta) = 0.224 + 0.776 \sin^{1.25}\theta \quad , \qquad 0 \le \theta \le 180°$$

These mathematical expressions for the element patterns can be used to simplify the calculations for the array patterns and directivity.

The equatorial plane patterns for the 42-in. diam satellite model with two antennas mounted 30 deg apart are shown in Fig. 28 based on the element patterns of Fig. 26. The effects of mutual coupling, reradiation from the cylinder, edge effects, and the radiation phase pattern of the individual elements were neglected in the computations. The array pattern is given by

$$E(\varphi) = E_e(\varphi)e^{jka \cos \varphi} + E_e(30° - \varphi)e^{j(ka \cos(30° - \varphi) + \delta)} \tag{5}$$

where

E_e = measured element patterns

k = $2\pi/\lambda$

a = phase center radius (assumed to be at the surface of satellite)

δ = phase delay

A102 - RUN 24

φ

0° 10° 20° 30° 40° 50° 60° 70° 80° 90°

RELATIVE POWER, dB

−10

−20

5 in.

800 MHz
600
450

·········· $E(\phi) = 0.224 + 0.776 \cos^{1.475} 0.75\phi$
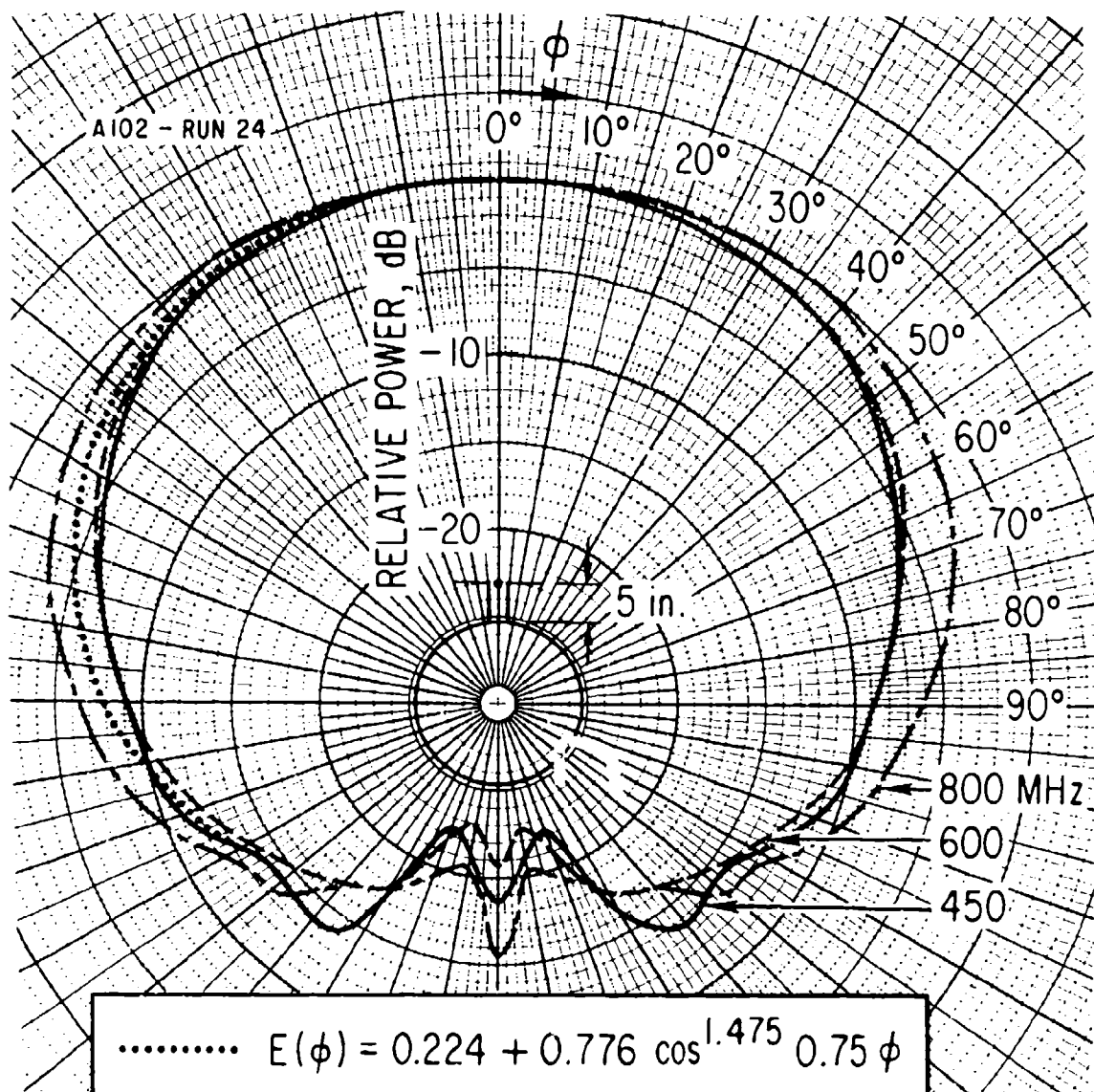
Figure 26.   Measured Element Patterns (Circular Polarization) of Crossed, Open-Sleeve Dipoles in the Equatorial Plane
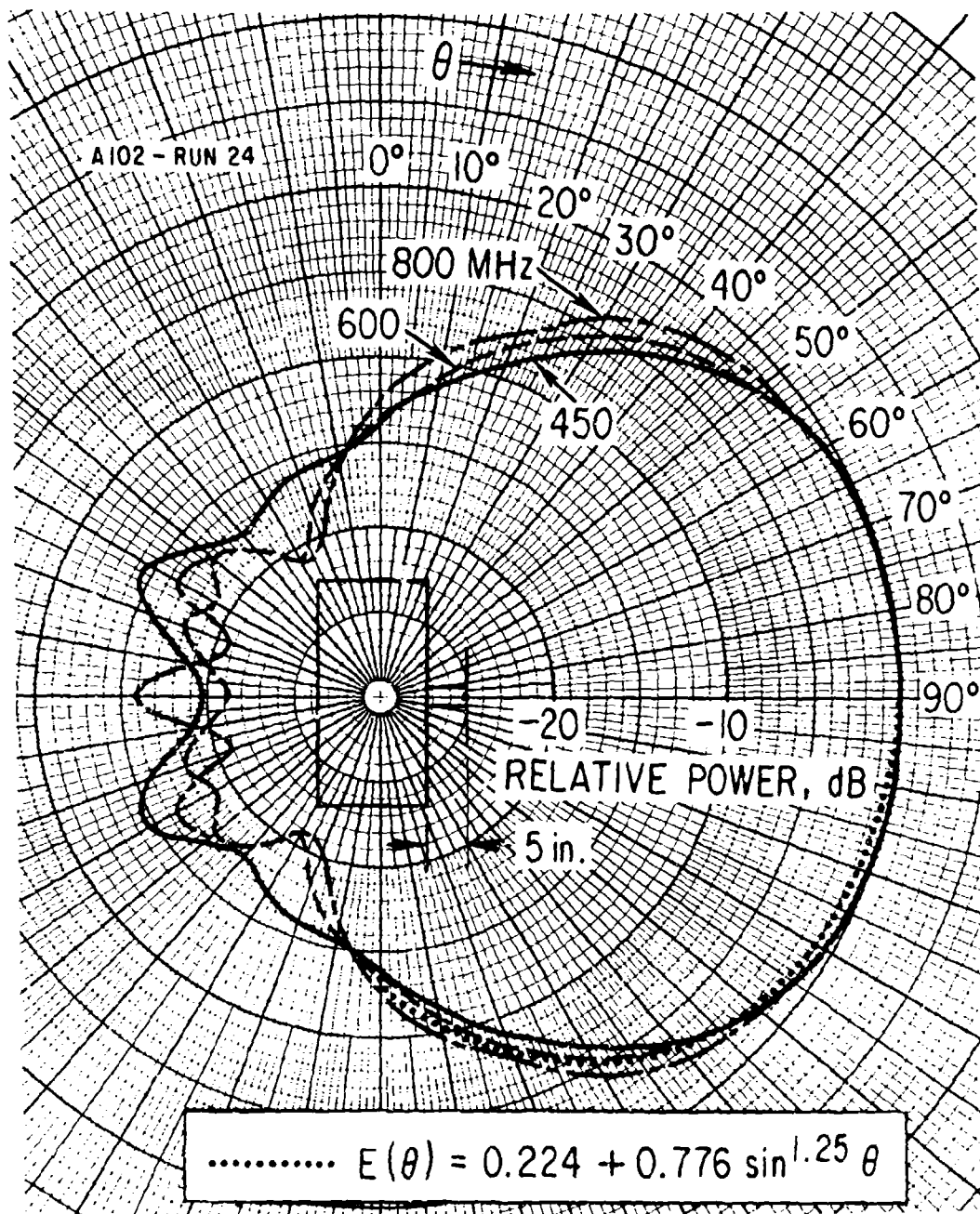
Figure 27. Measured Element Patterns (Circular Polarization) of Crossed, Open-Sleeve Dipoles in the Polar Plane
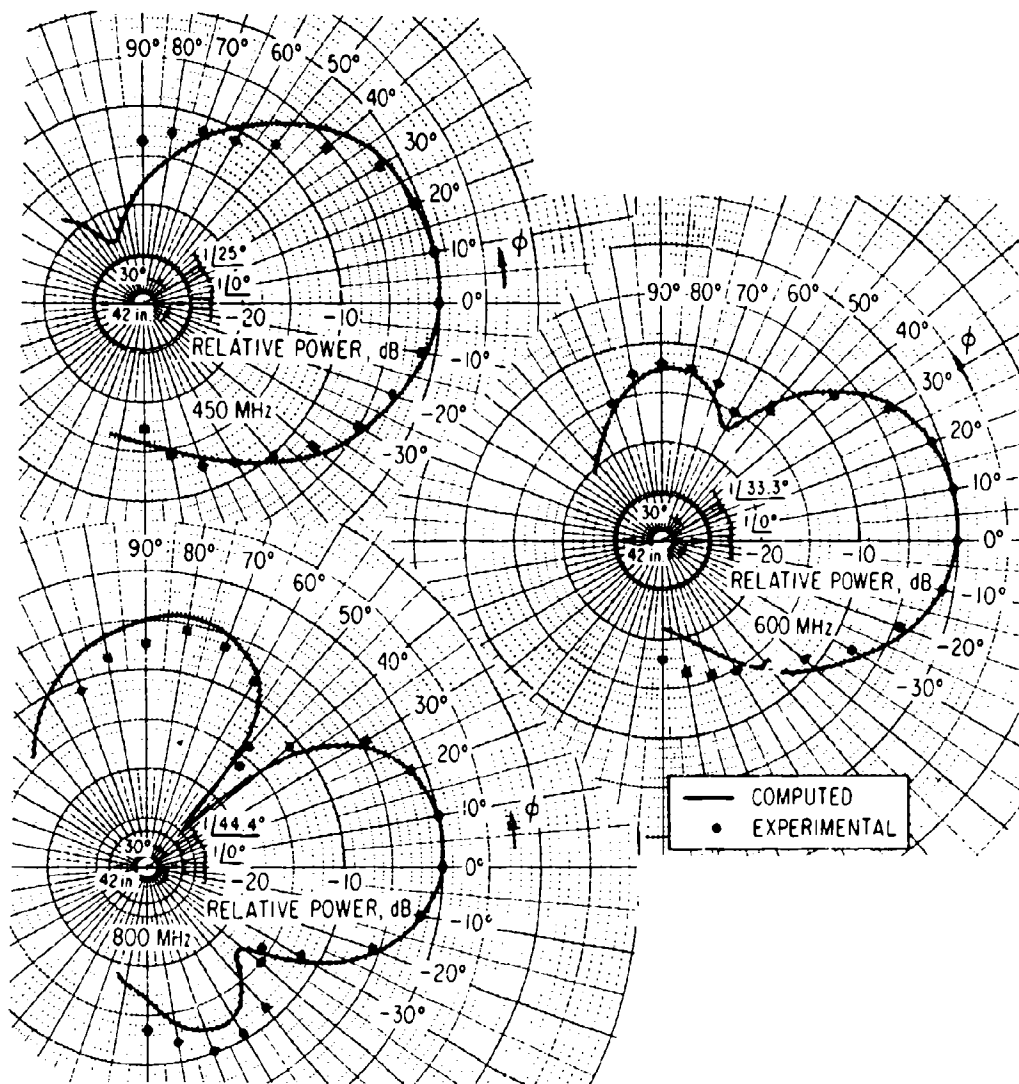
Figure 28. Computed and Measured Equatorial Plane Patterns

The phase delay δ is 25 deg at 450 MHz and since the phasing section is a coaxial cable, the phase at the other frequencies corresponds to the time delay in the cable. The pattern in the backlobe region is not shown because computations for pattern levels 15 to 20 dB below the beam peak would probably be unrealistic due to the assumptions that are made.

The experimental data points plotted in Fig. 28 permit comparison with the computed patterns. Relatively good correlation is shown in the main lobe and the sidelobe levels. The angular locations of the minima on the 600 and 800 MHz patterns indicate that the choice of the phase centers at the satellite surface is satisfactory. For the five patterns shown the experimental points have an average standard deviation of 0.25 dB within 3 dB of the main lobe peak and 0.57 dB in the remaining portion of the pattern. The standard deviation increases to 1.3 dB in the low-signal regions of the patterns. The data points are the average of from three to seven patterns such as those shown in Figs. 7 through 11. They represent the response to a circularly polarized wave and were obtained by taking the RMS values of the maximum and minimum amplitudes (major and minor axis of the polarization ellipse) at each aspect angle.

The radiation pattern in the polar plane (Fig. 29) corresponds to that of a broadside array of two elements fed in phase, or

$$E(\theta) = E_e(\theta) \cos\left(\frac{\pi s}{\lambda} \cos \theta\right) \tag{6}$$

where

θ = angle measured from the longitudinal axis of the satellite

$E_e(\theta)$ = measured element pattern

s = axial spacing of the elements

The experimental data points are superimposed on the computed polar patterns. Good correlation is shown in both the main lobe and the sidelobe
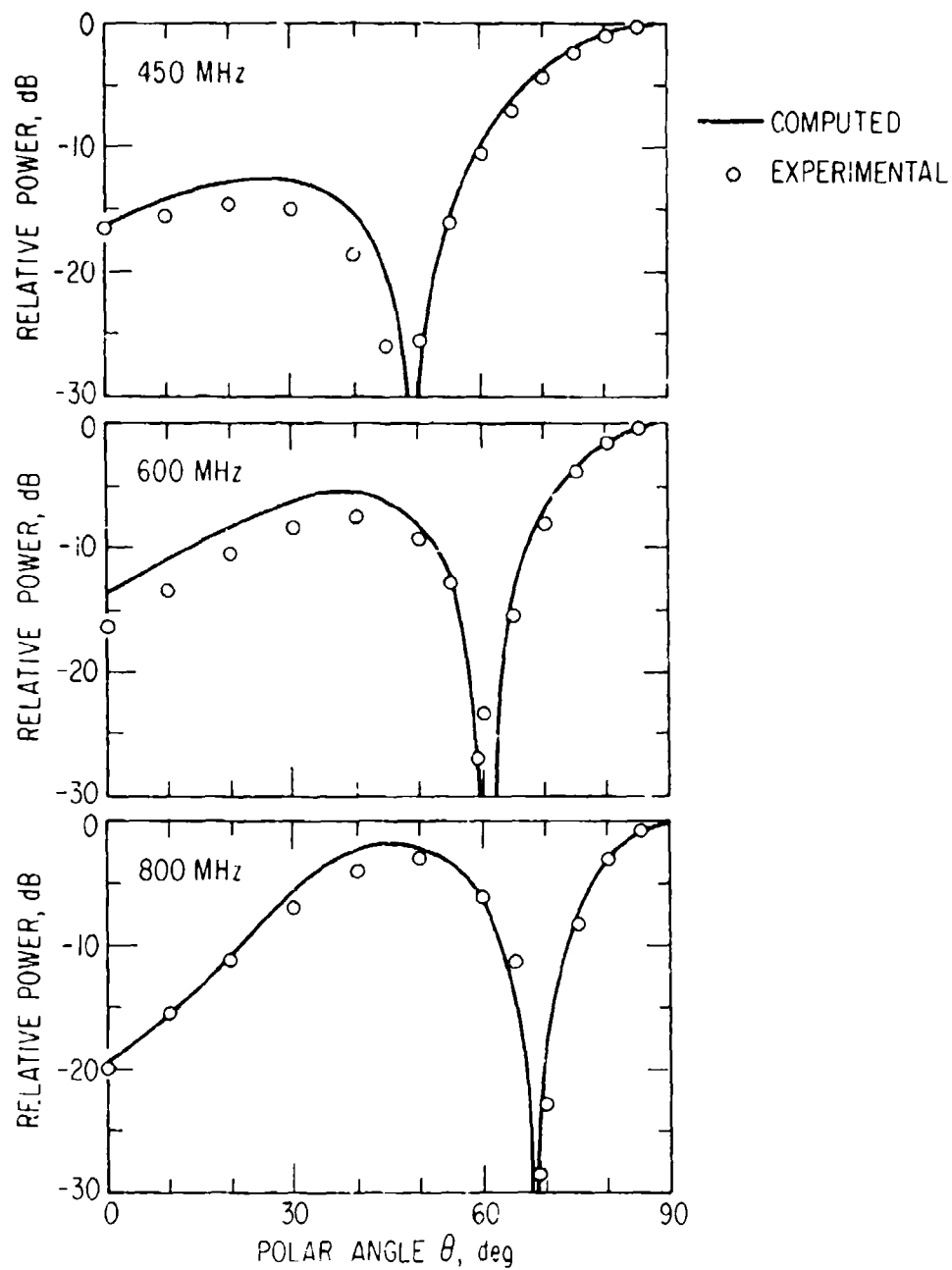
Figure 29. Computed and Measured Polar Plane Patterns
for an Axial Spacing of 20 in. Between
Crossed, Open-Sleeve Dipoles

levels. The experimental points have a peak deviation of ± 0.3 dB in the main lobe and generally within ± 0.5 dB in the remaining portion of the pattern except near the low-signal region. The patterns are shown for the angular region of θ = 0 to 90 deg because symmetry exists about θ = 90 deg. The data points represent the average of numerous patterns as well as the patterns in the range θ = 90 to 180 deg. The patterns were measured in a great circle cut through the azimuthal beam peak generally in the plane that contained the angle $\phi \approx 5$ deg.

The equatorial plane patterns were formed by the excitation of two antennas with a differential phase. Since the phasing section was a coaxial cable, the phase varied with frequency. The radiation pattern "ripple" or the gain decrease in the EOE direction (relative to beam peak) at the switching position is the factor that causes a severe reduction in the gain for the ϕ plane. The EOE ripple was determined from the equatorial plane patterns of Fig. 28. The EOE angles that correspond to switching positions S1 and S2 occur at ϕ = - 8.65 and + 23.65 deg (Fig. 1). The computed EOE ripple is shown in Fig. 30 as a function of the phasing between the two elements with frequency as a parameter. Optimum condition occurs when the phase delay corresponds to the intersection of the - 8.65 and + 23.65 deg curves of Fig. 30. However, since the phase delay varies with frequency, a compromise must be made in the selection of the phasing cable length. (The designer must select the phase that provides the optimum performance over the entire frequency band.) A comparison of computed and measured EOE correction values is given in Fig. 18 for both the polar and equatorial planes.

The directivity of the antenna was calculated from the computed patterns with $D = D_{V} D_{H}$ as described in Eq. (2). The results are compared with the measured values in Fig. 31.

B. VSWR AND MUTUAL COUPLING

The VSWR characteristics of the individual open-sleeve dipoles in the half-scale model were measured for various dipole-to-reflector spacings and

-44-

Figure 30. Computed Decrease in Gain at the Two EOE Positions for Equatorial Plane Patterns as a Function of Phase Delay
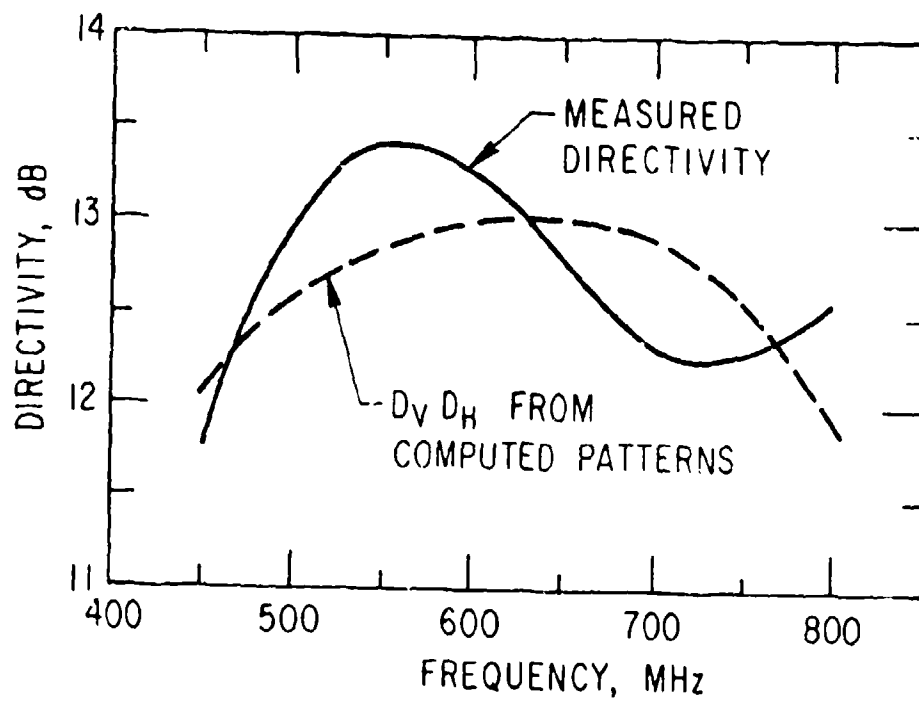
Figure 31. Measured Directivity as Compared With the Approximate $D = D_V D_H$ Relation

an axial dipole spacing of 20 in. The crossed dipole-pair NV_1 and NH_1 (Fig. 5) was selected for these measurements and all other dipoles in the array were terminated in a 50-ohm load.

The measured VSWR response of both the axial and transverse dipoles for several dipole-to-reflector spacings is shown in Fig. 32. In all cases, the overall VSWR response of the axial dipoles appears to be slightly better than that of the transverse dipoles. This is believed to be due to the difference in coupling effects. It should be mentioned that the VSWR of the individual dipoles in the half-scale model was greater than that for the full-scale model because the dipole diameters were not scaled exactly; i.e., the individual wire-grid dipoles used in the half-scale model array had an effective diameter of 0.481 in (Fig 4) although 1-1/8 in. is recommended for the full-scale model array (Fig. 35, Section IV). The VSWR characteristics of a full-scale wire-grid, flat-sleeve dipole are discussed in Section IV.

Coupling measurements were conducted on a group of four elements (2 × 2 array) excited for circular polarization. The magnitude of coupling was measured at the input port of each element with the other three excited and the remaining 20 elements in the array terminated in matched loads. A phasing cable with an equivalent phase delay of 25 deg at 450 MHz was used to provide a phase differential between the circumferential elements. The measurements were made in an anechoic chamber to reduce the effects from surrounding objects.

The measured coupling versus frequency for an axial dipole spacing of 22 in. is shown in Fig. 33. The reference reading was taken as the input power to one element. At each frequency, the circles represent the average coupling value of the four elements; the bars indicate the range of variations. On the average, the measured coupling ranges from about -16 dB at the low end of the frequency band to about -24 dB at the high end. The VSWR response at each element was also measured with the other three elements terminated in an open circuit, short circuit, or a matched load. No discernible change was observed.

○ AXIAL DIPOLE
△ TRANSVERSE DIPOLE
D_R DIPOLE-REFLECTOR SPACING
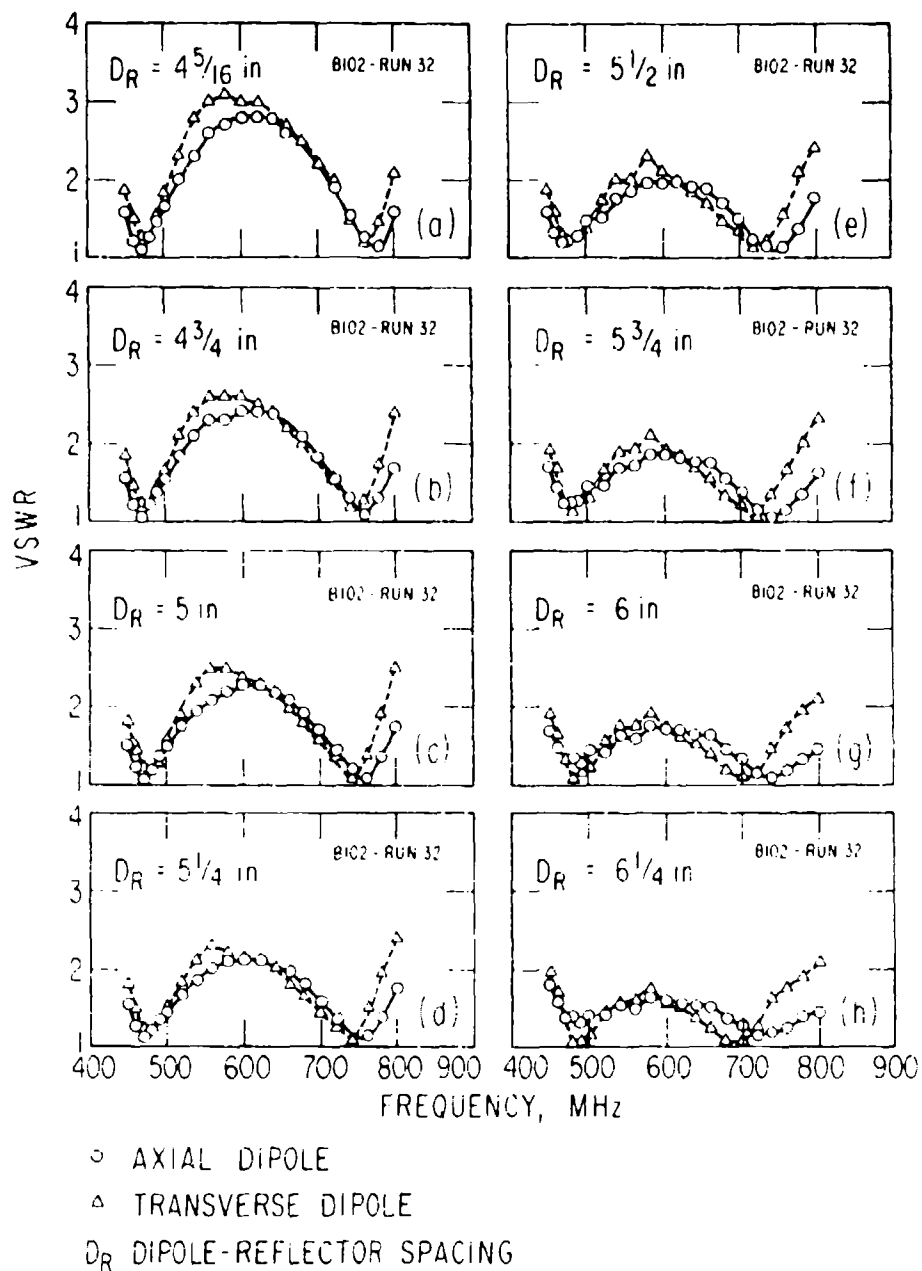
Figure 32. VSWR Characteristics of Individual Open-Sleeve
Dipoles in the Half-Scale Model Array for
Various Dipole-to-Reflector Spacings and an
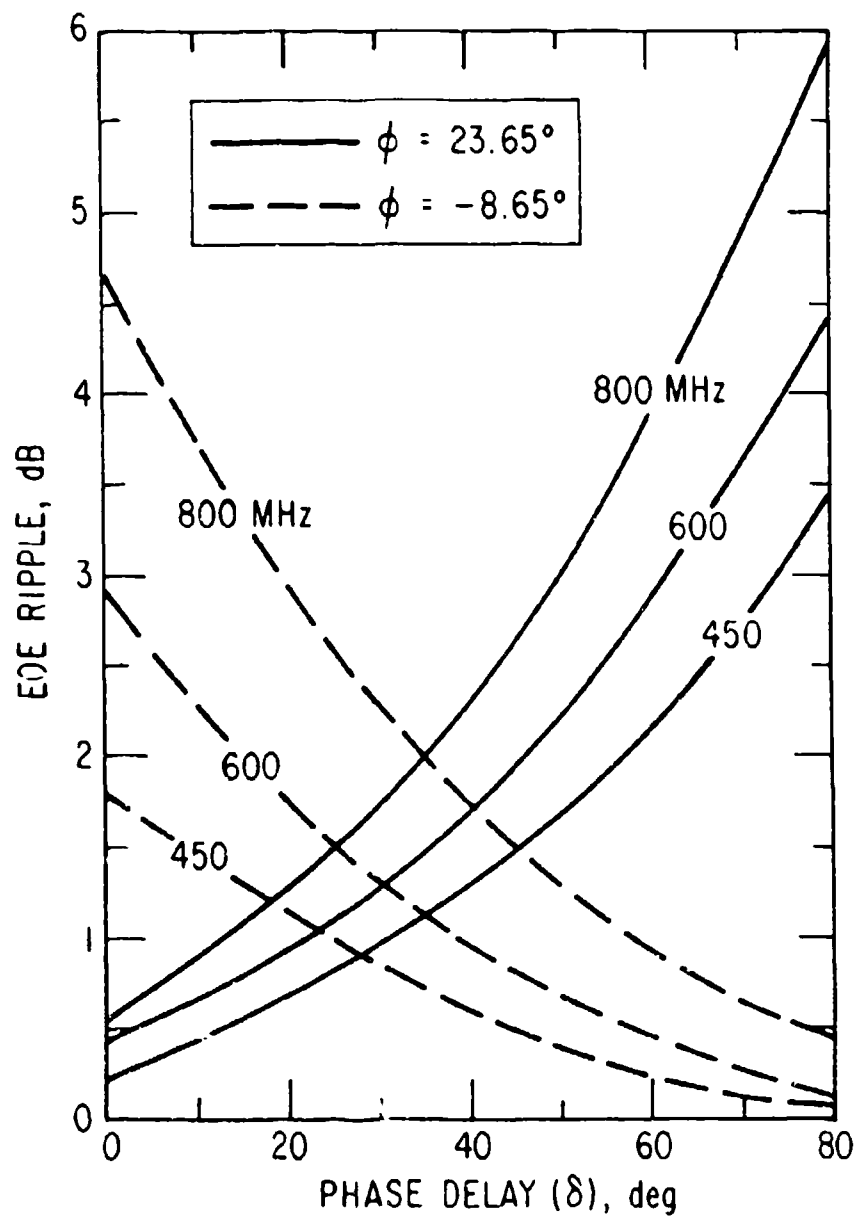Axial Dipole Spacing of 20 in.

-48-
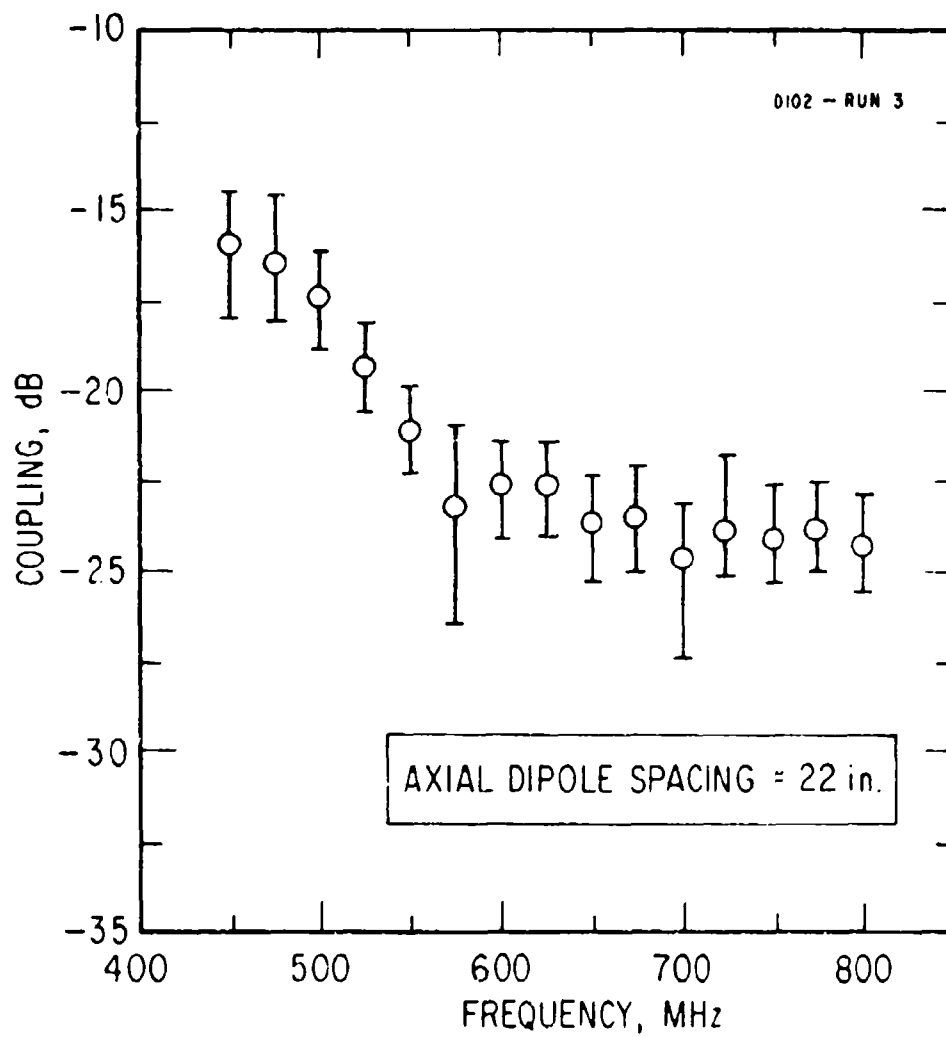
Figure 33. Measured Mutual Coupling as a Function of Frequency for an Axial Dipole Spacing of 22 in.

C. OTHER INVESTIGATIONS

1. SHADOWING

The objective of the wire-grid configuration was to minimize shadowing of the solar cells caused by the radiating elements. As previously mentioned, this construction simulates a metallic surface. The full-scale crossed, open-sleeve dipole mounted on a partial cylinder of approximately 84-in. diam is shown in Fig. 34. The effects of shadowing on the satellite surface are shown for two aspect angles. The dielectric supports for the dipoles and sleeves are constructed of lucite in order to simulate quartz in the final antenna. Shadowing is shown from all the edges. The dipole shadow reveals a minimum of four and as many as eight wires. The worst shadowing occurs from the balun, which produces a shadow as wide as 0.43 in. The holes for the dipoles and the slits for the sleeves would be eliminated in the final model. Instead, the wires would be passed through holes in the quartz material. This would reduce the shadowing by the dielectric edges.

The worst-case shadowing should be a consideration in the design of the solar cell array. The length of time the shadow persists, the time constant of the solar cell subsystem, the expected loss in power, and other deleterious effects should be investigated and methods established for resolving the problems.

2. OMNIDIRECTIONAL PATTERN FOR FAIL-SAFE MODE

As mentioned in Section IIA, the antenna system can be provided with a fail-safe mode of operation. Provisions can be made for switching the antenna to yield an omnidirectional pattern in the event of failure in the sensing, logic, and switching circuitry. System gain would naturally be less (6 to 10 dB) than normal. However, certain communication links would still be provided between the satellite and the high-performance terminals.

Preliminary equatorial plane pattern computations indicated a deviation from circularity of less than ± 0.3 dB at 225 to 300 MHz (full-scale) and

±1.5 dB at 400 MHz. If we assume that the pattern is omnidirectional, then the loss in directivity is the factor D_H described in Eq. (4) or the directivity of the array is equal to D_V (Fig. 25).
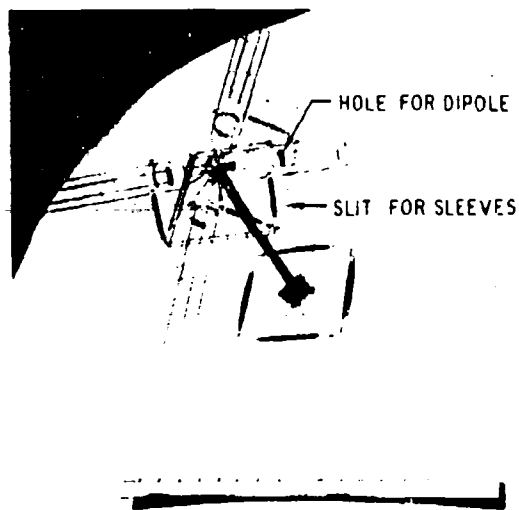
a. SUNLIGHT DIRECTLY OVERHEAD
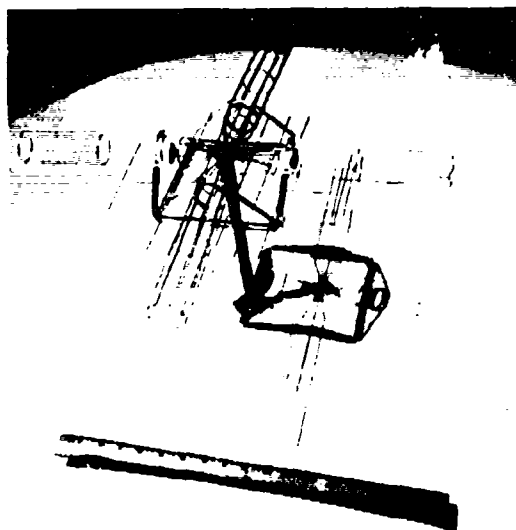
b. SUNLIGHT AT AN ANGLE

Figure 34. Photographs of Full-Scale Wire-Grid Dipole and its Shadow

-51-

IV. FULL-SCALE ANTENNA CONFIGURATION

A.   MECHANICAL CONSIDERATIONS

A brief study was devoted to the mechanical design problems associated with the full-scale antenna using an open-sleeve dipole as the basic radiating element. Although no comparison was made between the open- and conventional-sleeve dipoles, it appears that either should provide nearly equivalent electrical characteristics. In order to determine the mechanical advantages of the two sleeve dipole arrangements, an in-depth study would be required of all the launch, stowage, and space environments as well as fabrication techniques. The open-sleeve dipole was selected for the experimental work for the sake of ease in making adjustments of the antenna parameters and because of a simpler fabrication procedure. The present flat-sleeve dipole is an outgrowth of the initial study of crossed, open-sleeve dipoles, which used a tick-tack-toe sleeve arrangement (Ref. 3).

The dimensions of the full-scale wire-grid flat-sleeve dipole are shown in Fig. 35. A full-scale laboratory model was constructed for use in making VSWR tests and for studying the effects of shadowing (Fig. 34). The dipole is 20.2 in. long and consists of eight, 20-mil diam wires equally spaced on a 1.50-in. diam circle. The "wire cage," which simulates a solid metal surface, has an effective diameter of 1.13 in. The dimensions shown in Fig. 35 are considered to be nominal because some slight modifications may be required for optimization of the electrical characteristics.

In the recommended configuration, clear quartz is used for the sleeve supports in order to minimize shadowing of the solar cells. It is also recommended that the quartz edges have sharp corners in order to minimize the shadow area created from the edges. If desired, the sleeve can also be secured to the balun structure by a dielectric material. The dipole wires and sleeve wires are passed through the quartz material by way of 21-mil diam holes. The feed point vicinity demands special design considerations because it must be rigidly secured, and the copper and teflon portion of the

Figure 35. Full-Scale Wire-Grid Flat Sleeve Dipole Assembly

coaxial cable must be protected from the radiation environment. Thus, a quartz cylindrical cap filled with foam is suggested.

The balun consists of a coaxial feed section and a metal tube for the second arm. This tube should be used as the main mechanical support for the dipole assembly. Because there is a balun for each dipole, two structural tubes are available for the cantilever beam design.

Any additional supports that may be required for protection of the dipole assembly during launch were not considered in the present study. Furthermore, the concepts presented in Fig. 35 were given only a cursory evaluation in determining the survivability of the dipole assembly in a space and potential nuclear environment.

B.   ELECTRICAL PERFORMANCE CHARACTERISTICS

The electrical performance characteristics of a full-scale antenna are projected here on the basis of the results obtained from the half-scale model measurements. The basic radiating element is a crossed, wire-grid dipole with flat, open sleeves, although closed-sleeve dipoles may also be used and would probably provide equivalent electrical performance.

The VSWR characteristics of a full-scale laboratory model of a wire-grid dipole with flat sleeves are shown in Fig. 36. The dimensions are as given in Fig. 35. The measurements were made with the dipole mounted on a partial cylindrical surface of 84-in. diam (Fig. 34). The VSWR is less than 2.5:1 over the operating frequency range of 225 to 400 MHz. As mentioned in Section IIIB, the VSWR response of the full-scale model is flatter than that obtained for the half-scale model because the effective dipole diameter of the half-scale model is slightly less than half that of the full-scale model. However, the VSWR data of Fig. 36 indicate that the dipole and sleeve parameters have not yet been optimized and can be further improved. For example, the maximum VSWR of 2.5:1 at mid-band can be reduced by varying the length of the sleeves. The VSWR at the band edges will be slightly increased (Ref. 3), and a flatter VSWR response will be provided over the desired operating frequency band. However, this optimization procedure has not been performed because of the lack of time.
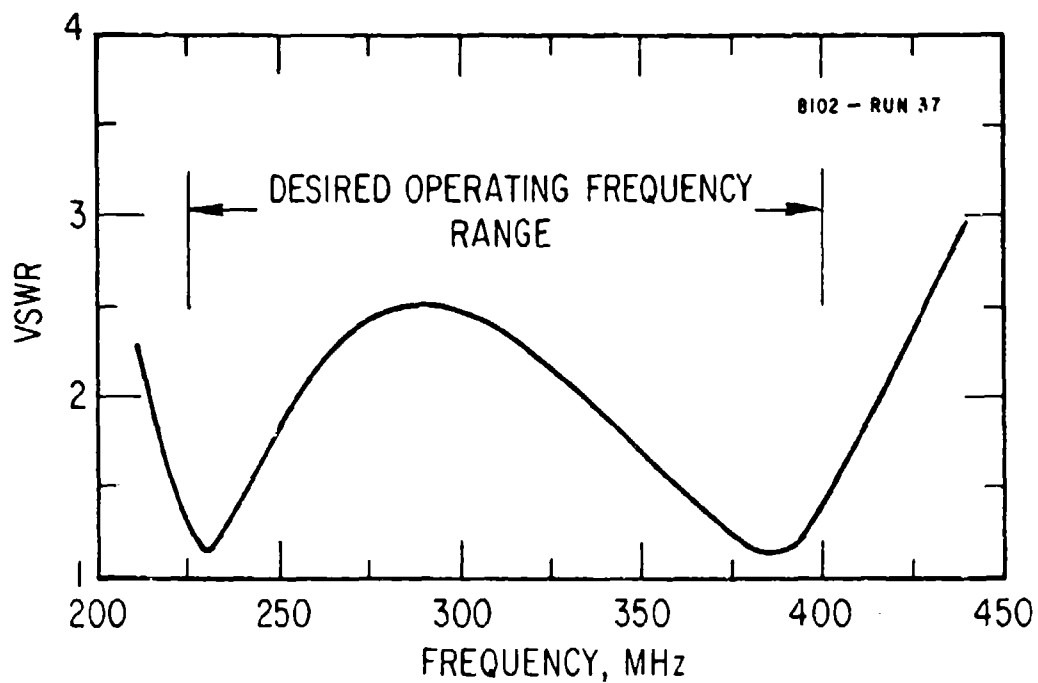
Figure 36. VSWR Response of a Full-Scale Wire-Grid Dipole With
Flat Sleeves. Cage diameter = 1-1/2 in.; effective
diameter = 1-1/8 in.

The radiation pattern characteristics of the full-scale antenna are expected to be identical to those of the half-scale antenna. The equatorial and polar plane radiation patterns at 225, 300, and 400 MHz are shown in Figs. 37 and 38, respectively. These patterns were obtained from the half-scale model measurements (Section IIIA). The axial dipole spacing is 40 in., and an azimuth phasing cable with an equivalent phase delay of 25 deg at 225 MHz is used. The corresponding phase delays at 300 and 400 MHz are 33 and 44 deg, respectively. The relative beam switching positions (S1 and S2) in the equatorial plane are also shown in Fig. 37. The decrease in gain at EOE is a measure of the pattern level relative to the beam peak at 8.65 deg from the beam switching positions. In the polar plane, the decrease in EOE gain is given by the relative pattern level at ± 8.65 deg from the beam peak. The decrease in gain at EOE as a function of frequency in the two planes is shown in Fig. 18.

The directivity of the full-scale antenna as derived from the half-scale measurements is given in Fig. 17. A comparison of the measured directivity with that obtained from 4π integration of the measured radiation patterns is also given. The difference is attributed to the antenna ohmic as well as other unaccountable losses. On the average, the antenna loss is 0.28 dB.

The antenna gain is obtained by subtracting the losses from the directivity. The estimated total antenna system losses (up to the diplexer input) are shown in Fig. 39 as a function of frequency. The various contributions are summarized in Table 4. The projected antenna gain (beam peak and EOE) for the full-scale antenna is shown in Fig. 40. The antenna meets the specified gain requirements delineated in Section IIA.

An exemplary feeding arrangement for the full-scale antenna is described in Ref. 11. The switching network is similar to that of the LES-6 antenna system (Ref. 12). A block diagram of the switching network is shown in Fig. 41. Since the system has 12 radiating elements around the circumference of the satellite instead of eight, SP6T switch elements are substituted in place of the SP4T switch elements used in the LES-6 system, and four switches are used. This arrangement reduces the power-handling requirement of the
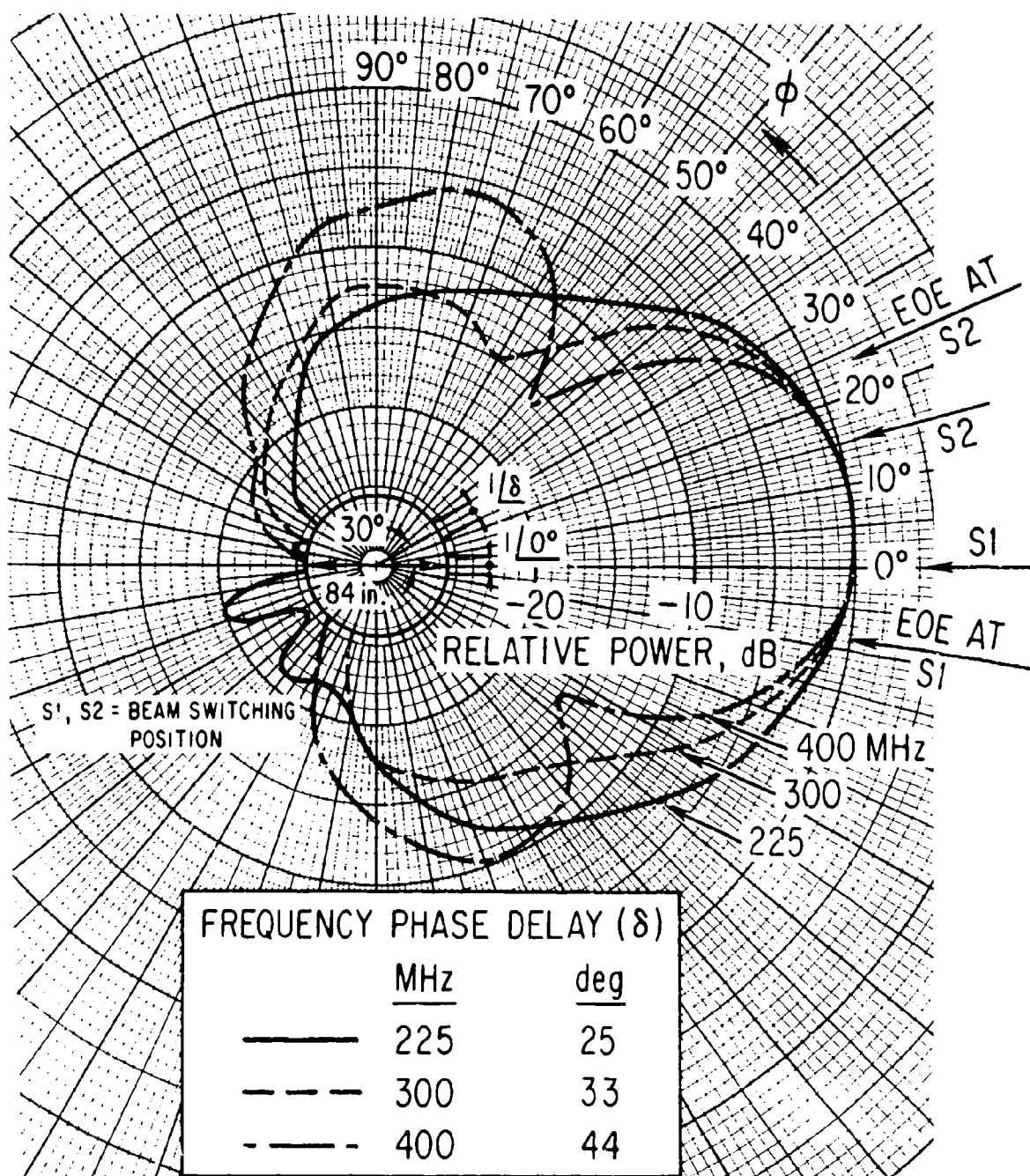
Figure 37. Equatorial Plane Radiation Patterns for 225, 300, and 400 MHz From Half-Scale Model Measurements
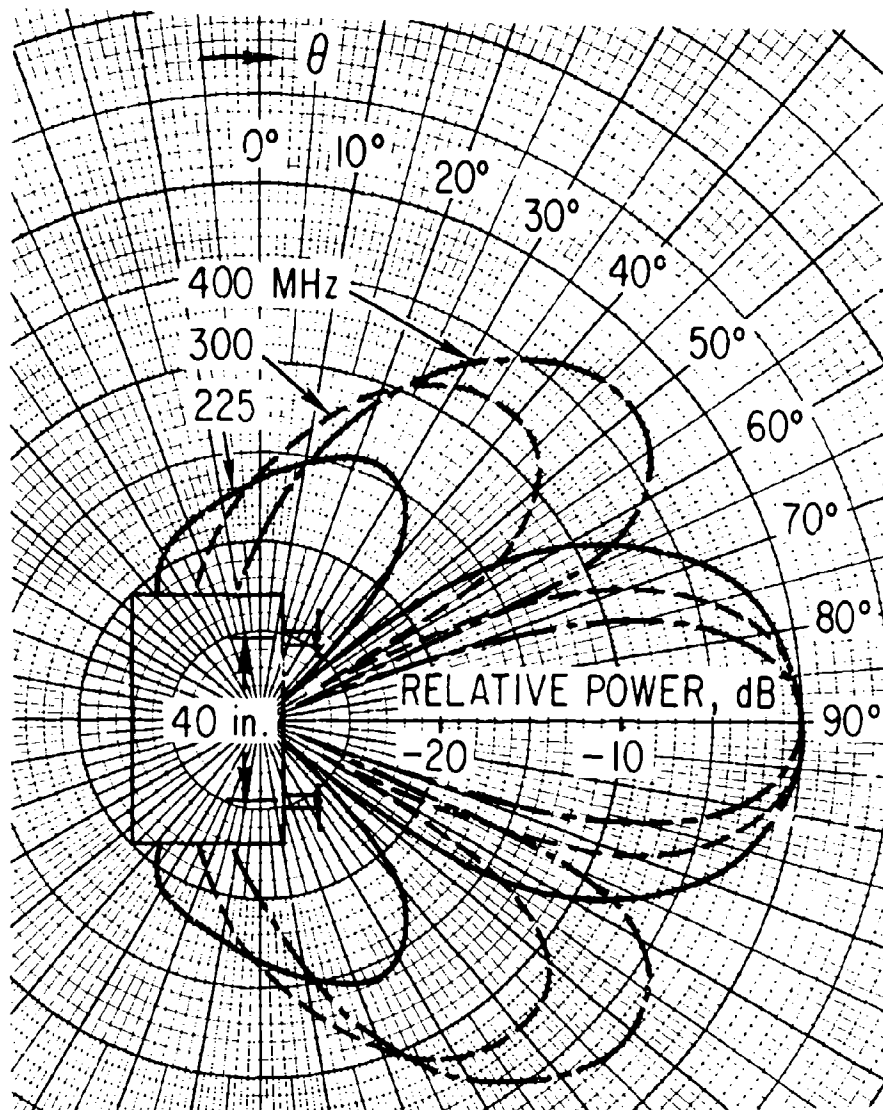
Figure 38. Polar Plane Radiation Patterns for 225,
300, and 400 MHz From Half-Scale
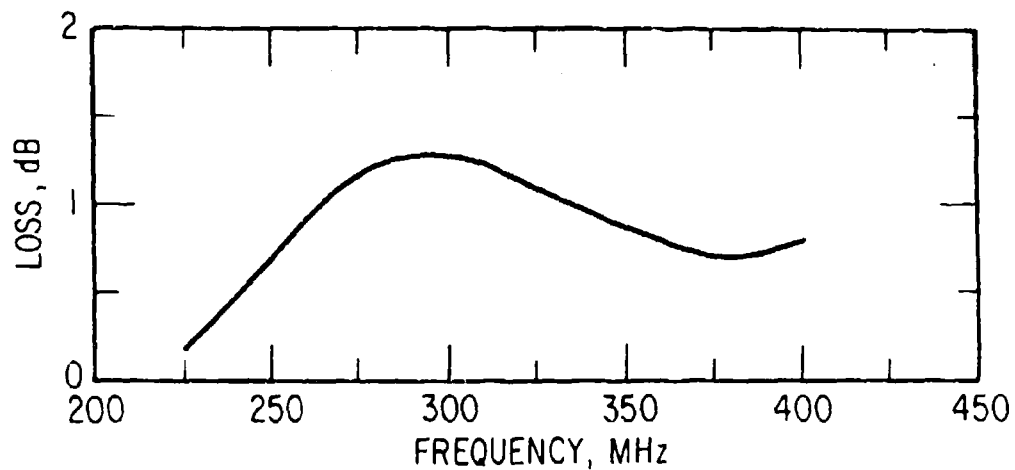Model Measurements

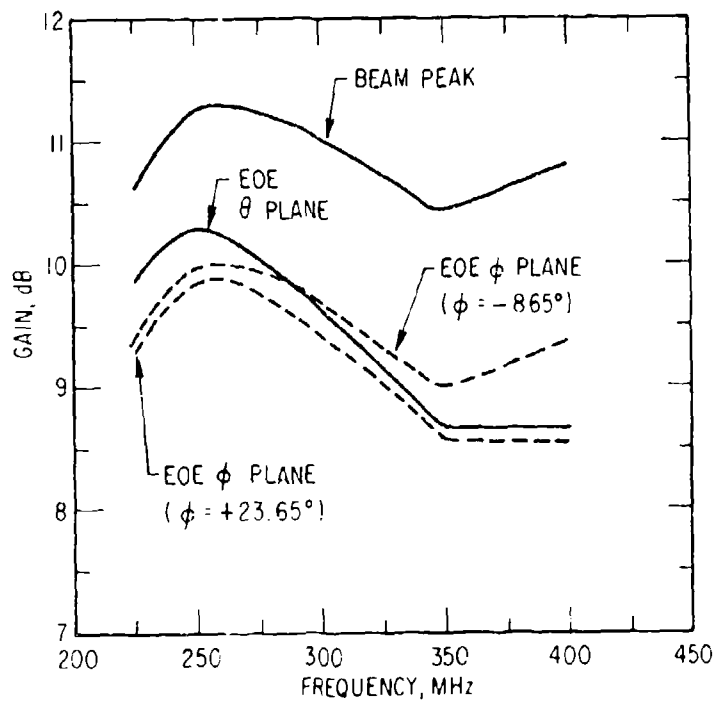Figure 39. Estimated Total Antenna System Losses for
Full-Scale Model

Figure 40. Gain as a Function of Frequency
for Full-Scale Model
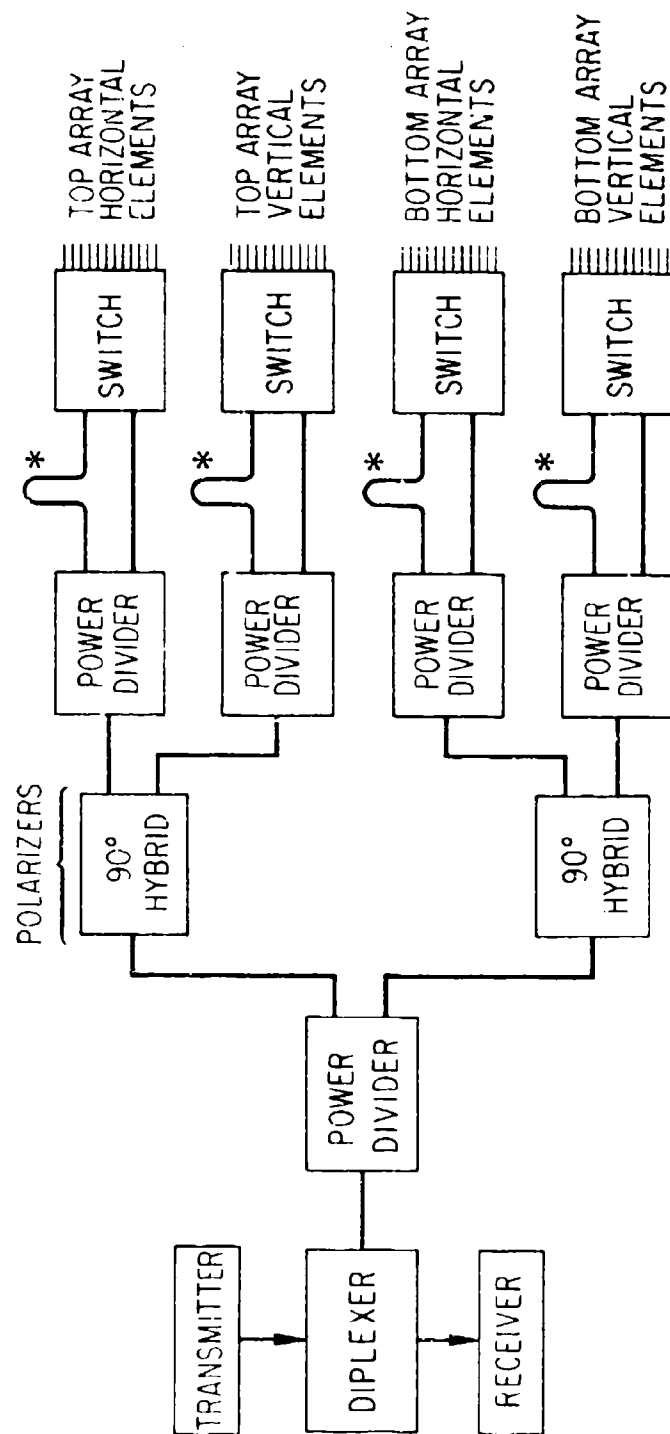
Figure 41. Block Diagram of Switching Network

individual switches, minimizes diode heating, and reduces the intermodulation level. The increase in weight from the use of four switches is offset by the fewer number of hybrids required for the overall feed network.

The power loss through the switching network for the antenna system is assumed to be the same as for the LES-6 system. The performance of a LES-6 backup switch (obtained from the MIT Lincoln Laboratory) was measured over the 225 to 400 MHz band and the results reported in Ref. 11.

Table 4. Summary of Antenna System Losses

Frequency, MHz	Losses, dB							
	225	250	275	300	325	350	375	400
Antenna	0.28	0.28	0.28	0.28	0.28	0.28	0.28	0.28
Mismatch	0.02	0.42	0.84	0.87	0.88	0.54	0.34	0.12
Polarizer	0.1	0.1	0.1	0.1	0.1	0.1	0.1	0.1
Switching Network	0.58	0.46	0.53	0.60	0.67	0.74	0.80	0.53
Power Combiners	0.2	0.2	0.2	0.2	0.2	0.2	0.2	0.2
Cables[a]	0.20	0.21	0.22	0.23	0.24	0.25	0.26	0.27
Total	1.18	1.67	2.17	2.28	2.07	1.91	1.98	1.50

[a] 12-ft length of 3/8-in. o.d. Styroflex or equivalent

V. SUMMARY AND CONCLUSIONS

A circularly polarized, electronically despun antenna system has been developed for use on spin-stabilized satellites at synchronous altitude. The antenna consists of 24 wideband radiating elements arranged to form two circular arrays of 12 elements equally spaced around the circumference of an 84-in. diam satellite. Only a 2 × 2 array is used at any one time. By means of electronic sequential switching and phasing, the beam can be scanned through 24 equally spaced positions about the spin axis of the satellite. A sensor-controlled switching logic can be used to point the beam toward the earth as the satellite rotates.

The basic radiating element is a crossed dipole with flat, open sleeves, and the antenna system is capable of operation over a frequency band of 1.8:1 (225 to 400 MHz). Both the dipoles and the sleeves are of wire-grid construction, which minimizes shadowing of the solar cells. For the experimental model, the measured VSWR of an individual dipole is less than 2.5:1 over the operating bandwidth.

The recommended switching network for the antenna system is similar to that used in the LES-6 system with slight modifications. Laboratory measurements of a LES-6 switch unit (obtained from the MIT Lincoln Laboratory) have indicated satisfactory performance over the entire 225 to 400 MHz band (Ref. 11).

Results of pattern and directivity measurements made on a half-scale model of the antenna system have indicated that the full-scale antenna can adequately meet the specified EOE gain requirements as summarized below.

	Goal	Achieved
225 - 250 MHz	9.0 dB	> 9.3 dB
250 - 400 MHz	6.0 dB	> 8.5 dB

REFERENCES

1. R. N. Assaly, M. E. Devane, B. F. LaPage, M. L. Rosenthal, and A. Sotiropoulos, LES-6 Antenna System, Technical Report No. 465, ESD-TR-69-43, DDC AD 693 197, MIT Lincoln Laboratory, Lexington, Mass. (10 March 1969).

2. M. L. Rosenthal, M. E. Devane, and B. F. LaPage, "VHF Antenna System for Spin-Stabilized Satellites," IEEE Trans. Antennas and Propagation AP-17, 443-451 (July 1969).

3. H. E. King and J. L. Wong, An Experimental Study of a Balun-Fed, Open-Sleeve Dipole in Front of a Metallic Reflector, TR-0172(2158)-3, The Aerospace Corporation, El Segundo, Calif. (25 August 1971); also, IEEE Trans. Antennas and Propagation AP-20, 201-204 (March 1972.

4. H. E. King and J. L. Wong, Wideband VHF-UHF Antenna Systems for Communication Satellites, TR-0172(2158)-2, The Aerospace Corporation, El Segundo, Calif. (3 February 1972).

5. E. L. Bock, J. A. Nelson, A. Dorne, "Sleeve Antennas," Very High Frequency Techniques, Ed. H. J. Reich, Radio Research Lab., Harvard University, McGraw-Hill Book Co., New York (1947), p. 123.

6. H. B. Barkley, The Open-Sleeve as a Broadband Antenna, Technical Report No. 14, DDC AD 82 036, U. S. Naval Postgraduate School, Monterey, Calif. (June 1955).

7. S. A. Schelkunoff and H. T. Friis, Antennas: Theory and Practice, John Wiley and Sons, Inc., New York (1952), p. 110.

8. R. B. Dybdal, H. E. King, J. L. Wong, and C. O. Yowell, Performance of a 90-Foot Quasi-Tapered Anechoic Chamber: 120 MHz to 93 GHz, TR-0059(6230-30)-4, The Aerospace Corporation, El Segundo, Calif. (3 September 1970).

9. A. Chlavin, "A New Antenna Feed Having Equal E-and H-Plane Patterns," IEEE Trans. Antennas and Propagation AP-2, 113-119 (July 1954).

10. H. E. King, J. L. Wong, and C. J. Zamites, Feasibility Study of Shaped-Beam Antennas for the Defense Communication Satellite Program, TDR-269(4111)-12, The Aerospace Corporation, El Segundo, Calif. (27 November 1964).

11.   R. B. Dybdal, D. G. Coder, and H. E. King, <u>LES-6 Antenna Switch
      Characteristics over the Extended Frequency Range of 225 to 400 MHz</u>,
      TOR-0172(2158)-7, The Aerospace Corporation, El Segundo, Calif.
      (15 November 1971).

12.   R. N. Assaly, <u>Development of UHF Switch for LES-6 Satellite</u>,
      Technical Report No. 473, MIT Lincoln Laboratory, Lexington, Mass.
      (4 December 1969).

DOCUMENT CONTROL DATA - R & D

(Security classification of title, body of abstract and indexing annotation must be entered when the overall report is classified)

1. ORIGINATING ACTIVITY (Corporate author)	2a. REPORT SECURITY CLASSIFICATION
The Aerospace Corporation El Segundo, California	Unclassified
	2b. GROUP

3. REPORT TITLE

225-400 MHZ ANTENNA SYSTEM FOR SPIN-STABILIZED SYNCHRONOUS SATELLITES

4. DESCRIPTIVE NOTES (Type of report and inclusive dates)

5. AUTHOR(S) (First name, middle initial, last name)

Howard E. King and Jimmy L. Wong

6. REPORT DATE	7a. TOTAL NO. OF PAGES	7b. NO. OF REFS
72 MAR 15	69	12

8a. CONTRACT OR GRANT NO.	9a. ORIGINATOR'S REPORT NUMBER(S)
F04701-71-C-0172	TR-0172(2162)-1
b. PROJECT NO	
c.	9b. OTHER REPORT NO(S) (Any other numbers that may be assigned this report)
d.	SAMSO-TR-72-77

10. DISTRIBUTION STATEMENT

Distribution limited to U.S. Gov't. agencies only; Test and Evaluation, 15 March 1972. Other requests for this document must be referred to SAMSO (SK).

11. SUPPLEMENTARY NOTES	12. SPONSORING MILITARY ACTIVITY
	Space and Missile Systems Organization Air Force Systems Command Los Angeles, California

13. ABSTRACT

A wideband, circularly polarized antenna system has been developed for use on spin-stabilized synchronous satellites. The satellite is assumed to be a right-circular cylinder of 84-in. diam and 77.3-in. height. The antenna consists of two circular arrays of 12 radiating elements equally spaced around the circumference of the satellite. The axial spacing between the two arrays is 40 in. The basic radiating element is a crossed dipole with flat open sleeves, and the VSWR is less than 2.5:1 over a 1.8:1 frequency band (225 to 400 MHz). Both the dipoles and sleeves are of wire-grid construction for minimization of solar cell shadowing. The electrical performance of the antenna is established on the basis of half-scale model measurements. It is shown that the antenna can provide an EOE gain (gain in the direction of the edge of the earth) of more than 9.3 dB from 225 to 250 MHz and at least 8.5 dB from 250 to 400 MHz.

DD FORM 1473

14	KEY WORDS

Sleeve dipoles

Open-Sleeve dipoles

Flat-Sleeve dipoles

Electronically despun antenna

Flat-Sleeve, crossed dipoles

Wire-Grid dipoles

Satellite antennas

Distribution Statement (Continued)

Abstract (Continued)